Solution-Phase Bulk Synthesis of Covalently Functionalized Black Phosphorus Nanosheets

Christine Haejung Chang

A thesis

submitted in partial fulfillment of the

requirements for the degree of

Master of Science

University of Washington

2019

Committee:

Alexandra Velian

Christine Luscombe

Program Authorized to Offer Degree:

Materials Science and Engineering

University of Washington

Abstract

Solution-Phase Bulk Synthesis of Covalently Functionalized Black Phosphorus Nanosheets

Christine Haejung Chang

Chair of the Supervisory Committee:
Assistant Professor Alexandra Velian
Department of Chemistry

Phosphorene—a two-dimensional layered semiconductor derived from the exfoliation of black phosphorus (BP)—is attracting significant interest in the nanomaterials community due to its high charge-carrier mobility, tunable bandgap, and anisotropic properties, but suffers rapid degradation upon exposure to ambient conditions. Herein we demonstrate the stabilization of phosphorene nanosheets *via* controlled chemical modification with organic azides, a relatively mild pathway towards covalent functionalization of the phosphorene surface, allowing for greater control over surface functionalization while preventing destructive phosphorene oxidation. Treated phosphorene exhibits a remarkable increase in ambient stability versus untreated phosphorene. This method offers further potential for the controlled, rational design of highly-tunable phosphorene-based materials using fundamental phosphorus chemistry as a guide.

TABLE OF CONTENTS

LIST OF FIGURES

LIST OF TABLES

ACKNOWLEDGEMENTS

First and foremost, I would like to thank my research advisor, Professor Alexandra Velian. Working for and learning from Alexandra has been an absolute privilege; she has been an extremely supportive mentor and I deeply appreciate her patience and understanding as I struggled to figure out where I want to be, both in science and in life. I am a better scientist and person for the time spent in her research group. Alexandra's vision, talent, and experiences as a scientist were a continual source of inspiration for me as a graduate student and have provided me access to many unique and wonderful opportunities in graduate school. I have always been, and continue to be, immensely honored to call myself a (now-former) member of the Velian group.

I would also like to extend my thanks to the Inorganic Division of the Department of Chemistry for providing a collaborative, intellectually stimulating environment through which to conduct chemistry. The supportive departmental atmosphere has contributed positively to my time here at UW. I am similarly grateful to the rest of the Department of Chemistry and Department of Materials Science and Engineering (MSE) students and staff, the Clean Energy Institute (CEI), Materials Research Science and Engineering Center (MRSEC), and Molecular Engineering and Materials Center (MEM-C). Collaborative research spaces such as the ones listed have made the University of Washington a truly outstanding institution at which to conduct research.

I also owe immense thanks to staff members at the University of Washington Molecular Analysis Facility (MAF), without whom much of the characterization work would not have been

possible. In particular, Dr. Micah Glaz has been invaluable in planning and troubleshooting various acquisitions. The staff and students maintaining MAF instrumentation have been superb.

I would also like to thank my thesis reading committee member and MSE co-advisor Professor Christine Luscombe, as well as the members of my prior qualifying exam committee (Professors Brandi Cossairt and Xiaodong Xu) for their razor-sharp questions and valuable feedback through their participation. I have enjoyed learning from all three of these brilliant faculty.

This work was completed in no small part through collaborations with soon-to-be Dr. William Holden and Professor Gerald Seidler in the Department of Physics, as well as Dr. Niri Govind at the Pacific Northwest National Laboratory. I am grateful for the time and resources volunteered towards advancing my understanding of my nanomaterials.

Of course, I must also thank my colleagues in the Velian group. In particular, I would like to thank the 2-D team—Kendahl Walz Mitra, a bright star who contributed to this work; Yuka Sakazaki, my laboratory partner-in-crime; and Dr. Daniel Tofan, a fountain of advice and manuscript edits—as well as the rest of the group (Jon Kephart, Ben Mitchell, and Andrei Chirila). I could not have asked for a better, nor more passionate, group of chemists. Between rigorous scientific discussions, mutual late-night grinds, Group Lunch™, glovebox jam sessions, and general shenanigans, our lab family has been an irreplaceable part of my experience here at UW. (This includes past members Andrew Boggiano, Muammer Yaman, and Elizabeth Ramirez.)

Last (but never least), I would like to thank my family, who constantly overwhelm me with the depth of their support. I warmly thank my aunt, Susan Dible, for always being proud of and staying invested in my educational endeavors. To the rest of my family, my brother Peter, my sister Catherine, and my parents Charles and Sung: I cannot find words powerful enough to thank you. You are the very foundations of my soul; I could not have become who I am today without you.

Chapter 1. INTRODUCTION

Since the advent of graphene, interest in two-dimensional (2D) materials has rapidly grown due to promising applications in next-generation nanotechnology applications. The size-dependent properties of 2D nanosheets inherently allows tuning of their inherent optoelectronic properties, such as the optical bandgap. Modification, both *via* covalent and noncovalent interactions, opens further avenues towards doping, solubility, band gap engineering, and interfacial engineering.[1]

In the class of 2D materials, exfoliated black phosphorus (BP), also known as phosphorene, is an appealing next-generation electronic material for a variety of reasons. For instance, phosphorene exhibits high carrier mobility on the order of 1,000 $cm^2V^{-1}s^{-1}$, with a calculated mobility of up to 10,000 $cm^2V^{-1}s^{-1}$, which is comparable to supported graphene.[2–4] The optical bandgap of exfoliated BP further reveals wide tunability accessed through *n*-layered phosphorene, from 2.1 eV for monolayer ($n = 1$) phosphorene to 0.3 eV for bulk ($n = \infty$) BP, which spans a range of energies larger than other 2D materials which absorb in the visible or near-infrared (NIR) region.[2,5,6] Considered in conjunction with a favorable current on-off ratio (above 10^5)[4] and strong anisotropic response (e.g. optical, conductive, and mechanical),[7,8] BP offers tantalizing potential for novelty and high-performance in the realm of nanoelectronics.

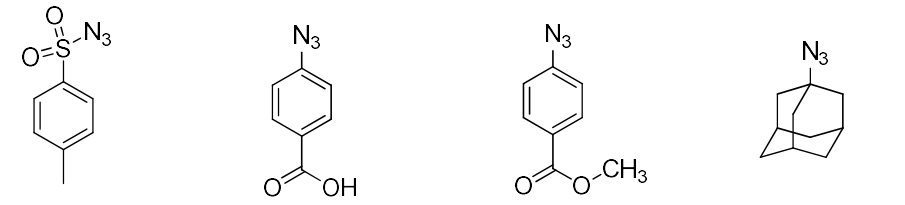

However, the broader application of phosphorene is hindered by its high susceptibility to ambient oxidation into amorphous P_xO_y species. In this report, we describe a general approach for

the covalent functionalization of phosphorene by treatment with a family of organic azides R–N_3 (R = tosyl, –$SO_2(C_6H_4)CH_3$; methyl benzoate, –$C_6H_4C(O)OCH_3$ and adamantyl, –$C_{10}H_{15}$). The presence of new covalent bonds on the surface of the nanosheets was corroborated *via* multiple characterization techniques. X-ray photoelectron and emission spectroscopy (XPS and XES) analysis indicates that about half of available surface atoms participate in new bonding interactions. Vibrational (infrared and Raman) spectroscopy analysis as well as measurements with energy dispersive X-ray spectroscopy (EDS) suggest the transfer of R group functionalities onto the nanosheets, as well as changes in P–P bond vibrations due to new bonds on the basal plane. Chemical modification is also supported by imaging techniques (scanning electron and atomic force microscopy). Through controlled functionalization of phosphorene nanosheets, this work opens an avenue for the design of performance-optimized materials which balance stability with favorable optoelectronic properties.

1.1 Covalent Modification of Black Phosphorus

Black phosphorus (BP) is comprised of trivalent phosphorus atoms which form a plane of puckered phosphorus atoms in an orthorhombic lattice (Figure 1). In the bulk material, these planes (phosphorene monolayers) are held together *via* strong interlayer interactions, which must be disrupted in order to exfoliate the phosphorene surface.[2,9] Though BP is the most thermodynamically-stable allotrope of elemental phosphorus, it is easily oxidized under ambient conditions. The process of ambient oxidation is ultimately destructive to BP, consuming the characteristic corrugated lattice of P atoms in favor of various amorphous phosphorus oxides and phosphoric acid derivatives.[10–12]

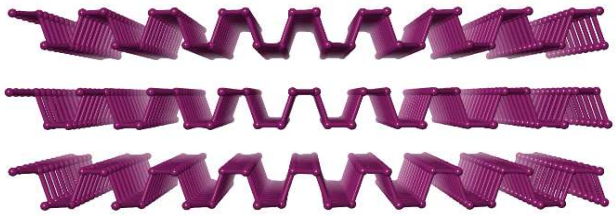

Figure 1. Side-on view of black phosphorus (BP).

While the poor ambient stability of phosphorene—which quickly degrades into phosphorus oxides (P_xO_y) under exposure to ambient conditions—has been a challenge in phosphorene research, this property also exposes the potential of phosphorene to readily form covalent bonds on its surface. During the ambient oxidation of phosphorene, the trivalent phosphorus atoms comprising the structure are readily activated to form P-O and P=O bonds, either terminally to form stable phosphorus oxides or through σ-bond insertion to form unstable P-O species.[11,13] Isoelectronic bonds between phosphorus and other elements (carbon, for instance) may be similarly accessible, and depending on the reactive precursor, may prevent σ-bond insertion to selectively form stable surfaces.

The covalent functionalization of phosphorene has been reported in single-flake studies with aryl diazonium[14] salts and in bulk reaction studies with aryl iodonium[15] precursors to form P-C bonds using the in-situ generation of carbenes. The resultant materials exhibit increased ambient stability without the destruction of the underlying phosphorene lattice. However, these highly reactive diazonium salts present harsh reaction conditions. Indeed, previous reports suggest the formation of a thick organic layer on the surface of phosphorene rather than a controlled activation of surface sites.[15]

Recently, Yang *et al.* reported the thermolytic treatment of phosphorene with 4-azidobenzoic acid. The authors propose a reaction occurs through in-situ generation of nitrenes through thermal activation of the azide group, leading to the reactive species which activates phosphorene.

In the formation of P-N bonds, milder reagents such as organic azides can be used. These azide precursors can photolytically generate nitrene species. We envision 3 possible binding

motifs: the Staudinger reaction ("terminal"), σ-bond insertion (e.g. cleavage of a P-P bond in favor of P-N-P), and bridge formation (e.g. P-N-P bridge formation).

1.2 THE STAUDINGER REACTION

The Staudinger reaction, first described in 1919 by the eponymous chemist, proceeds through the reaction between an azide (R-N_3) and a phosphine (PR'$_3$) to ultimately form an iminophosphorane (R-N=PR'$_3$) *via* extrusion of gaseous N_2 (Scheme 1).[16] The reaction was shown to proceed through the initial formation of phosphazides (R-N_3–PR'$_3$). Though some phosphazides have been isolated through careful selection of the phosphine and azide involved (e.g. electronic or steric stabilization),[17–21] at low temperature,[22] or as ligands in inorganic complexes,[23] the majority of phosphazides undergo rapid extrusion of N_2 and formation of the corresponding iminophosphorane. The reaction proceeds *via* an intramolecular cyclization to a four-membered N_3P intermediate, and generally its rapidity renders the phosphazide difficult to isolate.

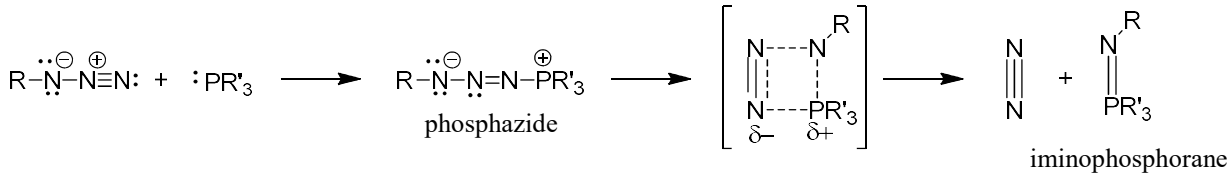

Scheme 1. Mechanism for the Staudinger reaction of phosphines with azides.

The chemical properties of phosphorene, such as its nucleophilicity and the resultant stability of the corresponding phosphazide has not yet been reported in literature. Recent work by Yang *et al.* reports the functionalization of phosphorene with organic azides The chemistry of phosphorene itself, and potential energy barriers to the formation of expected products due to its rigid structure, are not fully understood. A more detailed discussion of potential reaction pathways is presented in Section 1.4.

1.3 Photolytic Reaction Between Phosphines and Azides

Under photolytic conditions, azides are known to dissociate into reactive nitrenes, primarily as triplet nitrenes in the case of aryl azides (Scheme 2).[24,25] With the addition of nucleophilic phosphines (in this case, phosphorene), the presence of a relatively electron-deficient nitrogen such as a nitrene may offer a direct pathway to the formation of a P–N bond. For example, the nitrene may react with the phosphorus nanosheets to form "iminophosphorene" (P_n=NR'), as observed for most molecular phosphines. Alternatively, the nitrene may bridge two phosphorus atoms P–N–P either by insertion into a P–P bond, or by connecting two adjacent, but not directly bonded P atoms.

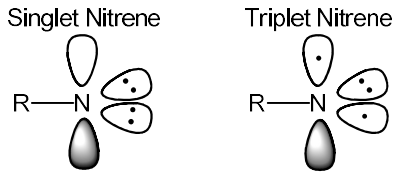

Scheme 2. Representation of a singlet and triplet nitrene, which may be formed from azides under photolytic conditions

1.4 Reaction Pathways and Products Formed Between Phosphorene and Azides

Black phosphorus (BP) structurally resembles an extended phosphine network, though its chemical reactivity in that regard has not been studied. The traditional Staudinger reaction and the subsequent formation of an iminophosphorane product discussed above is the product expected for molecular phosphines.

For phosphorene, the extended phosphorus atom network brings about two additional possible reaction pathways in reaction with molecular azides. In one case, the NR fragment could insert into the P–P bond to form a P–N–P bond. This type of insertion is precedented for molecular diphosphanes[26] and bears resemblance to the insertion of oxygen atoms into white phosphorus

(a highly unfavorable process with an energy of combustion >700 kcal/mol).[27] In translation to BP, insertion of N to cleave P–P bonds would significantly disrupt the lattice structure.

In the second case, the nitrogen atom binds with two P atoms which are 3 atoms apart in the armchair direction. This results in the formation of a P–N–P bridge across a phosphorene "trench" in a manner similar to that which forms destructive bridging P–O–P bonds under ambient degradation pathways.

In a reaction with organic azides, BP could engage in multiple types of bonding interactions with the NR fragment, such as the three (or a combination thereof) discussed above.

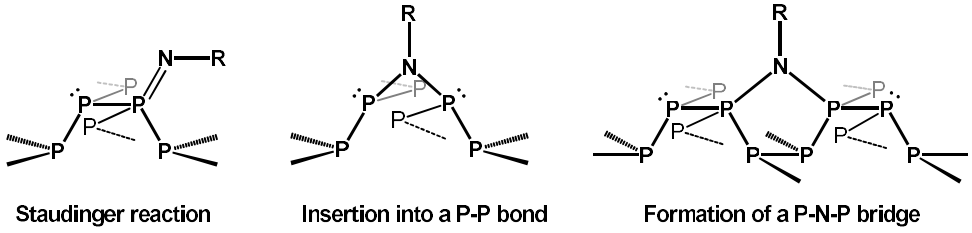

Scheme 3. Three proposed reactions between phosphorene and organic azides.

Pristine phosphorus atoms in BP have a formal oxidation state of 0. In a bond with nitrogen atoms, the phosphorus is converted to a higher oxidation state; thus, the reaction is a process by which phosphorus is oxidized. To avoid confusion with oxidation *via* oxygen to produce phosphorus oxides, reaction with nitrenes will be described as "functionalization," whereas degradative oxidation in the presence of water and oxygen will be referred to as "oxidation," though both are formally oxidative processes from the perspective of involved phosphorus atoms.

Chapter 2. CHARACTERIZATION OF EXFOLIATED BLACK PHOSPHORUS (*EXF*-BP)

Exfoliated black phosphorus (*exf*-BP) was prepared *via* liquid phase exfoliation in benzonitrile (PhCN). Concentrations of exfoliated nanosheets generated through the process was quantified *via* the method described by Warren *et al.* using UV-vis spectroscopy.[28] Using this method, the average concentration was determined to be 320 ± 90 μg/mL (10 ± 3 mM) across 7 separately-produced batches. To verify the morphology of the exfoliated material, scanning electron microscopy (SEM) and atomic force microscopy (AFM) were used to image dispersed

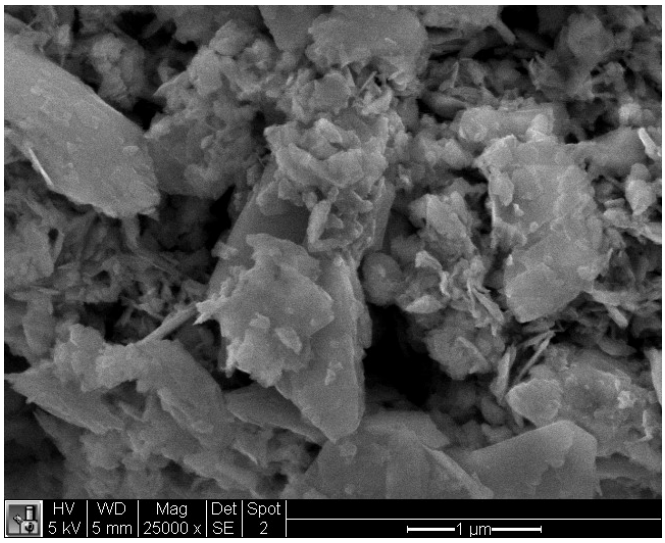

Figure 2. Scanning electron microscope (SEM) image of exfoliated BP. The *exf*-BP layers show some aggregation due to high-speed centrifugation processing.

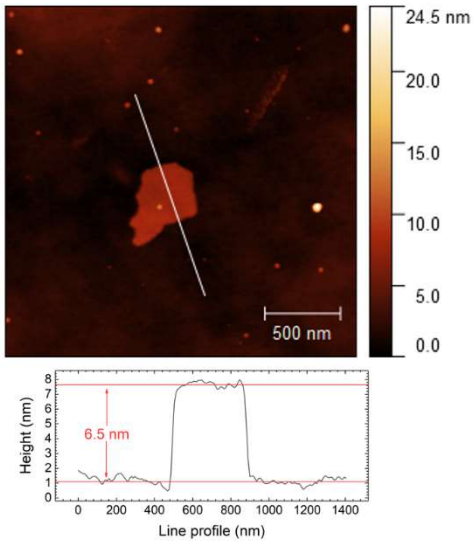

Figure 3. Atomic force microscope (AFM) image of an exfoliated BP flake, dropcast from bulk preparation.

flakes of BP (Figure 3, Figure 2). The distribution of sizes is also apparent in wider-zoom AFM images (not shown), though small and few-layered BP flakes are still observed. Powder x-ray diffraction (XRD) of the exfoliated material verifies the presence of the (020), (040), and (060) signals of black phosphorus reported in literature (Figure 4a).[5] The relatively broad peaks speak

to the exfoliated nature of the nanosheets. Absorption spectroscopy in the UV-vis-NIR reveals a broad absorption in the visible range and a slight shoulder at ca. 450-500 cm^{-1}, consistent with literature reports of the absorption profile of exfoliated BP (Figure 4b).[28]

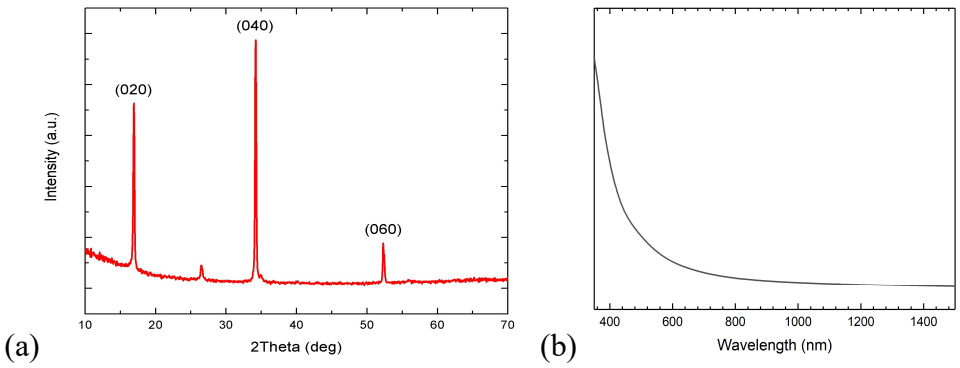

Figure 4. (a) Powder X-ray diffraction (XRD) spectrum acquired for *exf*-BP. Notably, the spectrum was acquired under ambient conditions. The characteristic diffraction peaks of black phosphorus are preserved in the exfoliated material. (b) X-ray powder diffraction pattern for exfoliated, unreacted black phosphorus.

2.1 Raman Spectroscopy

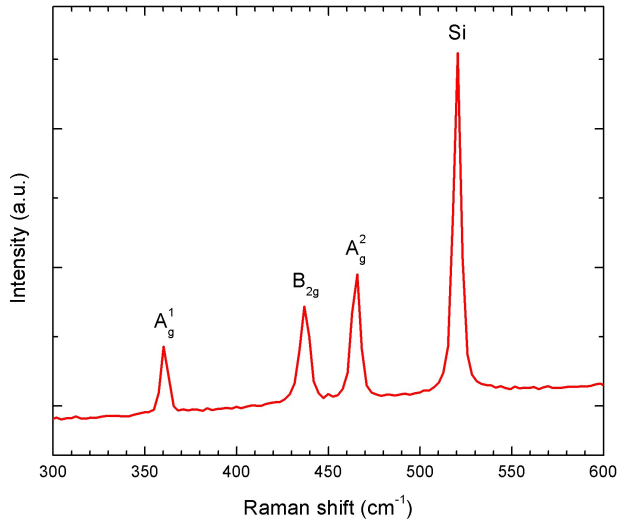

Figure 5. Raman spectrum (λ = 514 nm) of exfoliated black phosphorus, with normal Raman modes indicated.

The integrity of as-produced *exf*-BP was also characterized *via* Raman spectroscopy, X-ray photoelectron spectroscopy (XPS), and X-ray emission spectroscopy (XES). The Raman spectrum of exfoliated BP shows the characteristic A_g^1, B_{2g}, and A_g^2 modes of black phosphorus matching those observed in literature (Figure 5). Height ratios between the three peaks indicate the presence of few-layered BP, and the ratio between A_g^1 and A_g^2 ranges between 0.48 – 0.60 across various batches (where $A_g^1/A_g^2 < 0.4$ - 0.6 has been previously noted as an indicator of pristine, unoxidized BP).[13]

2.2 Infrared Spectroscopy

Infrared (IR) spectra of untreated *exf*-BP, using both attenuated total reflectance (ATR-IR) and diffuse reflectance measurements, reveals only very weak signals ranging from 1000-1100 cm^{-1} (Figure 6). The observed signals potentially indicate low levels of oxidized P_xO_y species (P-O and P=O signals are known to appear in this region).

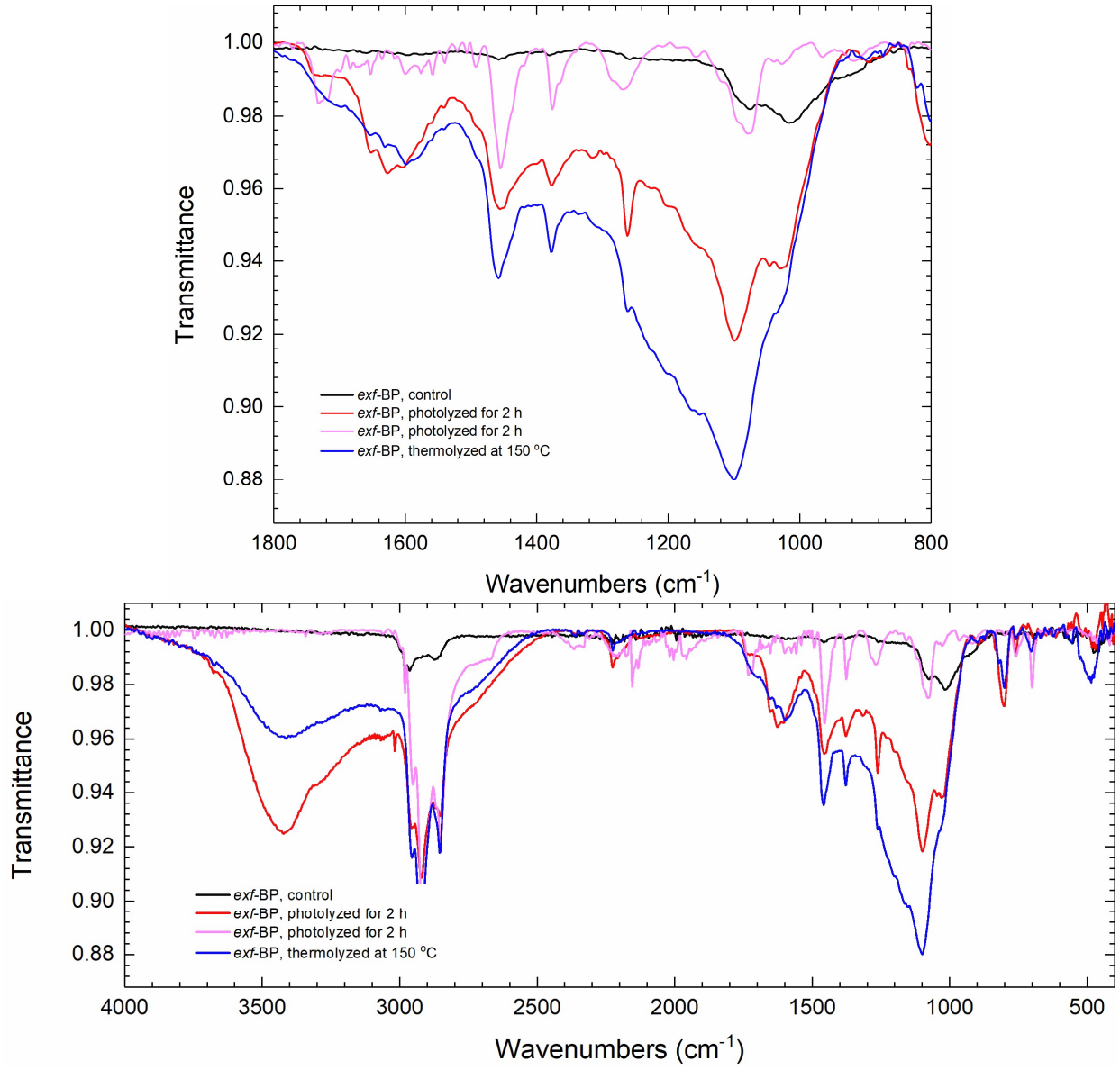

Figure 6. (top) Infrared (ATR-IR) spectrum of washed *exf*-BP, zoomed from 800–1800 cm^{-1}. (bottom) Full zoom from 400–4000 cm^{-1}. All treatments (photolysis, thermolysis) were performed on *exf*-BP solutions produced in PhCN. Signals from P–O are apparent at *ca.* 1100 cm^{-1} for all treatments. Note that the red and blue traces were measured using DRIFTS, versus the black and pink traces measured *via* ATR-IR; the two analysis types lend different signal-to-noise ratios, and DRIFT spectra possess a broad signal at 3400 cm^{-1} indicative of residual water from the KBr. Signals at 500, 700, 750, 1400, 1450, and 2230 cm^{-1} are residual solvent signals from PhCN.

2.3 X-RAY PHOTOELECTRON SPECTROSCOPY (XPS) AND X-RAY EMISSION SPECTROSCOPY (XES)

The P 2p core level XPS spectra of pristine, untreated *exf*-BP show the expected P $2p_{3/2}$ and P $2p_{1/2}$ components at 130 eV as well as minimal oxidation (~0%) of the surface, indicated by the presence of P-O (~132-134 eV) on the sample (Figure 7). Though P-O is not evident in the pristine *exf*-BP sample, analysis of *exf*-BP after 2.5 d ambient exposure is illustrative (Figure 9).

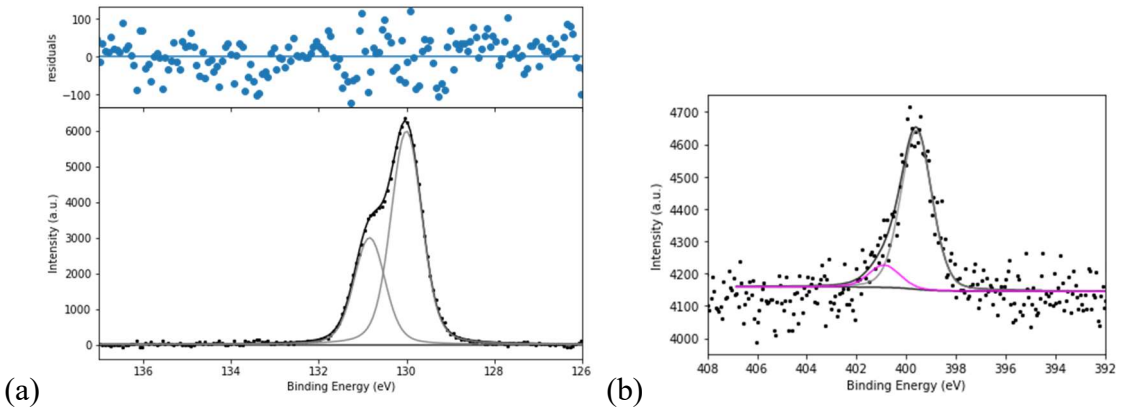

(a) (b)

Figure 7. (a) XPS P 2p high-resolution spectrum for the *exf*-BP depicted in the survey spectrum (Figure 8), along with residuals plot illustrating the fit. No phosphorus is oxidized during the exfoliation process. Relatively uniform residuals scattering indicates good fit to the acquired data. (b) XPS N 1s high-resolution spectrum for the same sample of *exf*-BP. The signals observed at 399.6 eV (88%) and 400.9 eV (12%) are similar to literature reports of N 1s signals for benzonitrile chemisorbed and physiosorbed to a Si substrate (399.8 eV and 400.2 eV, respectively).[29]

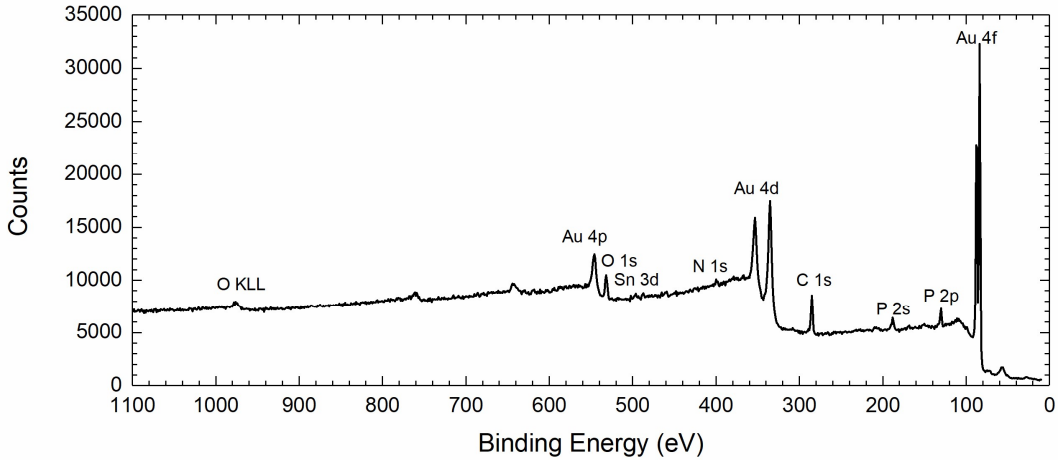

Figure 8. XPS survey spectrum of *exf*-BP drop-cast onto an Au-coated substrate.

Table 1. Relative composition, based on XPS survey spectrum, of *exf*-BP drop-cast onto an Au-coated substrate. Atomic composition percentages are weighted by the relative sensitivity of XPS to each element.

XPS Line	Adjusted B.E. (eV)	Atom %
C 1s	285.0	42.3
Au 4d5	335.1	34.8
P 2p	130.1	10.2
O 1s	532.1	12.7

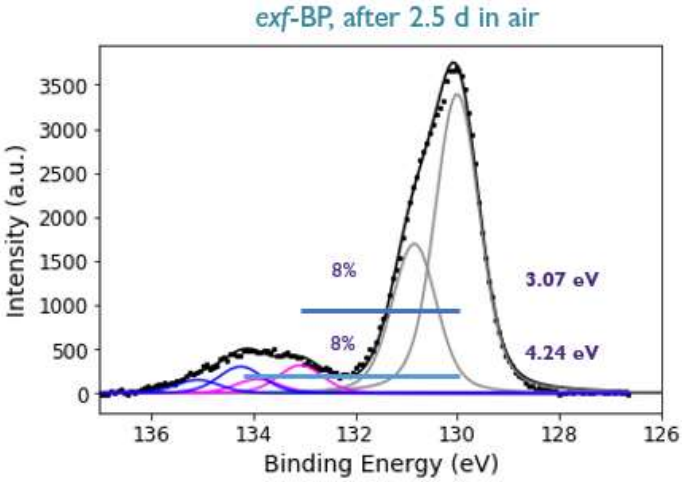

Figure 9. XPS P 2p high-resolution spectrum of *exf*-BP after 2.5 d ambient exposure.

Phosphorus Kα emission spectra were analyzed using linear combination fitting with the nonlinear least-squares fitting Python package LMFIT.[30] Spectra were fit with two spectral peak

shapes, each consisting of two Voigt profiles representing the $K\alpha_{1,2}$ doublet. The widths and intensity ratios of these peak shapes were constrained to the values obtained from fitting unmodified phosphorene and Na_2HPO_4 reference compounds, and the energy positions of the peak shapes were allowed to vary. The residuals in the fitting procedure were weighted assuming Poisson statistics. The speciation of the samples was then calculated from the relative intensity of the fitted components.

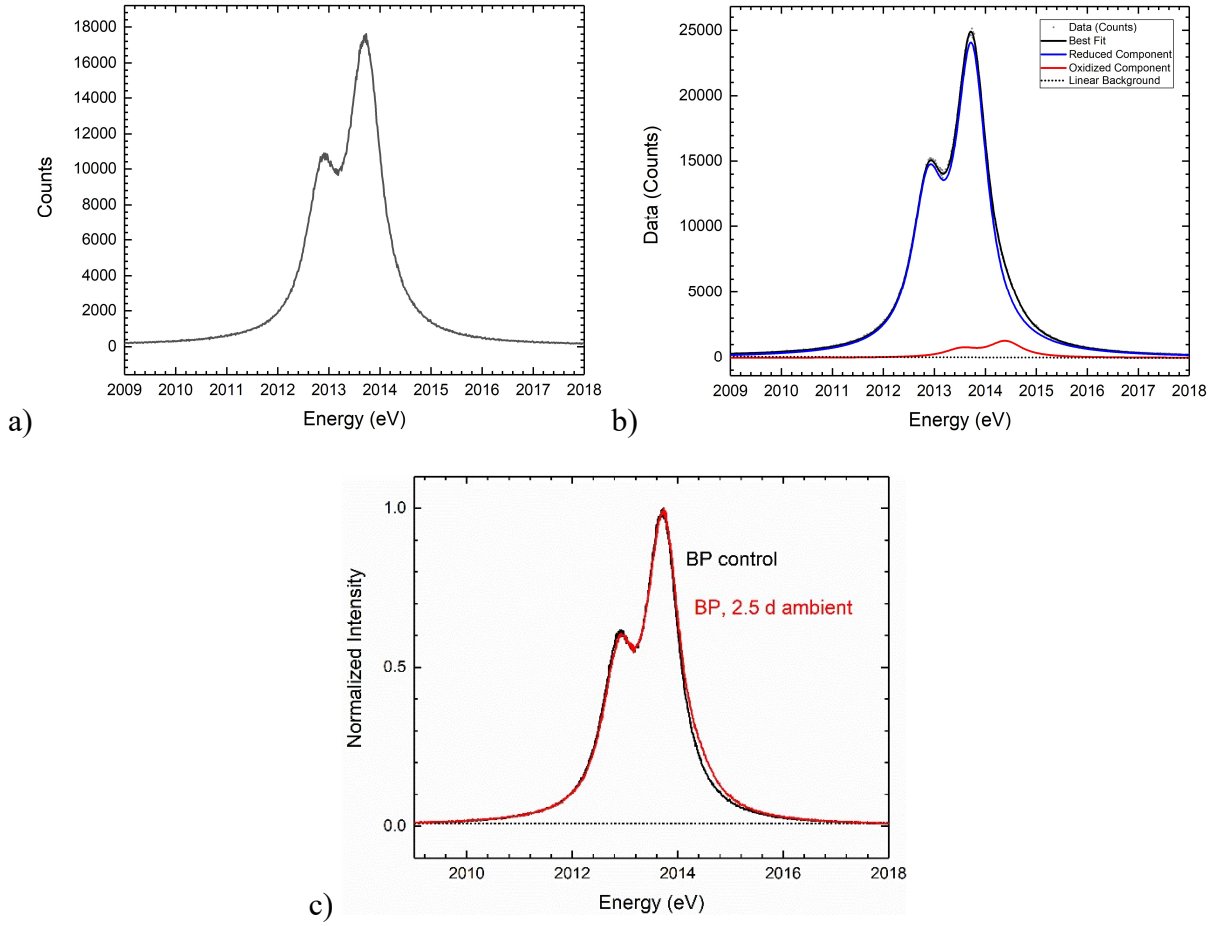

Figure 10. (a) X-ray emission spectrum (XES) for the P Kα signal for pristine *exf*-BP showing no detectable oxidized phosphorus signals using least-squares fitting. (b) P Kα for of a sample of *exf*-BP after exposure to ambient conditions for 2.5 days. In this sample approximately 5% of the P Kα signal can be attributed to an oxidized component using least squares fitting. (c)

Overlay of P Kα signals for the *exf*-BP spectrum from part (a) in black, against the sample exposed to ambient conditions (b) in red.[1]

The two components of the fitting procedure represent the phosphorus atoms of the unperturbed phosphorene substrate (the more reduced component) and the phosphorus atoms whose oxidation state has been affected by modifications (the more oxidized component). The P Kα XES signal for phosphorene can be fit to a single oxidation state component at 2013.71 eV identified as the Kα emission of unoxidized *exf*-BP with >99% certainty ($\chi^2 = 1.06$), indicating that little detectable P-O resides within the bulk of the sample (Figure 10).

Phosphorus 2p XPS signals were analyzed using the procedure detailed in Section 5.1.2. The signal corresponding to higher-oxidation-state P atoms is deconvoluted into separate P 2p signals with fixed widths. The oxidation state of P_xO_y species produced from ambient oxidation can be probed *via* the shift in binding energy to a higher oxidation state in XPS. For *exf*-BP after 60 h exposure to ambient conditions, a significant increase in the contribution from P-O (from 0% to 16%) is observed. The same oxidation is observed *via* XES, where 5% of the P Kα signal is attributed to a second P Kα oxidation state component at 2014.4 eV arising alongside the BP Kα at 2013.7 eV. Note that the nature of XPS leads to greater sensitivity towards surface atoms compared to measurement *via* XES, which samples a much greater depth of the sample for bulk analysis. XES directly probes fluorescence arising from valence- to core-shell relaxation, while XPS which detects valence electrons emitted through ejection; thus, unlike XPS, XES is not affected by potential scattering of the electrons ejected deeper beneath the surface of analyzed material. The identified proportion of oxidized P is thus lower in XES than in XPS for the same material (5% vs. 16%, respectively). Oxidized BP was also characterized through Raman

[1] X-ray emission spectra were acquired and subsequently analyzed by William Holden in Gerald Seidler's research group at the University of Washington. Results are included with permission.

spectroscopy, where the A_g^1/A_g^2 indicative of oxidized P was found to be 0.75-0.85, versus ca. 0.5 for pristine BP. The drastic change in A_g^1/A_g^2 is consistent with literature reports using the peak height ratio to characterize the extent of oxidation for BP, though we note in literature the ratio is observed to decrease rather than increase. It is possible that prior studies normalized Raman spectra in a manner we did not replicate.

2.4 CONCLUSION

A reproducible procedure for the production of exfoliated black phosphorus (*exf*-BP) was established, and the characterization of *exf*-BP nanosheets confirmed adherence to literature reports. The many of the techniques used to characterize *exf*-BP establish a known reference point for spectroscopic comparison against covalently modified *exf*-BP.

Chapter 3. THERMOLYTIC TREATMENT OF *EXF*-BP WITH ORGANIC AZIDES

Chemical functionalization of BP was performed through the direct addition of organic azides to suspensions of exfoliated BP prepared in PhCN. The Staudinger reaction of molecular phosphines typically proceeds under mild conditions, e.g. at room temperature on the order of minutes or a few hours.[16,31]

Based on the general rapidity of molecular Staudinger reactions even at room temperature, mild reaction conditions were initially probed for the analogous Staudinger reaction with BP. The organic azides screened were tosyl azide (TsN_3), benzoic acid azide ($BA\text{-}N_3$), and adamantyl azide (AdN_3), selected for their range of reactivities (*i.e.* more reactive azides $R\text{-}N_3$ feature stronger electron-withdrawing R groups). The azides were combined with exfoliated BP first at room temperature for several hours, and then under heating at 70 °C for 16 h in PhCN. Treated BP was isolated *via* filtration through PTFE membrane filters and washed several times with various solvents to remove contaminants, unconsumed reactants, or degradative byproducts (see Chapter 5 for more details).

3.1.1 *Thermolytic Treatment of* exf-*BP with AdN_3, TsN_3, and 4-Azidobenzoic Acid (BAN_3)*

After treatment with AdN_3 (70 °C, 16 h), the isolated *exf*-BP was primarily analyzed *via* XPS and Raman spectroscopy. In the core-level P 2p XPS spectrum, apart from the BP P 2p signals, signals from $P_{1,2}$ are observed (Figure 12). The lower magnitudes of $P_{1,2}$ in comparison to $P_{1,2}$ from ambient oxidation points towards a P state on the surface which is less strongly oxidized than P=O and P-O bonds. The data is consistent with the formation of a bond between P and N. Attenuated total reflectance infrared (ATR-IR) spectroscopy confirms the absence of $\upsilon_{as}(N_3)$ =

2083 cm^{-1} in treated BP, indicating the total consumption of the reactive N_3 group in the bound organic groups as well as the absence of residual starting material in spectroscopic analysis.

Using infrared (IR) spectroscopy, tosyl azide exhibits a strong asymmetric N_3 stretching mode $\upsilon_{as}(N_3)$ at 2130 cm^{-1}. The absence of this signal in the DRIFT spectrum of treated material is accompanied by sulfonyl S=O signals at 1377 and 1152 cm^{-1} (*vs.* 1367 and 1158 cm^{-1} in free TsN_3), supporting the presence of tosyl groups on the surface of BP (Figure 11).

The XPS spectrum acquired in the P 2p spectra region of TsN_3-treated BP under mild heating reveals $P_{1,2}$ values of 3.2 eV, which is significantly lower than $P_{1,2}$ for P_xO_y species formed through ambient oxidation of phosphorene described previously ($P_{1,2}$ = 3.7 eV) (Figure 12). The oxidation state of the new signal is similar to that observed in AdN_3-treated BP. The two separate azide treatments thus produce new features consistent with a P=N or P-N bond.

BP treated with benzoic acid azide was analyzed *via* diffuse reflectance infrared Fourier-transform (DRIFT) spectroscopy, also known as DRIFTS. The spectrum of treated *exf*-BP reveals the persistence of the asymmetric azide peak $\upsilon_{as}(N_3)$ = 2115 cm^{-1}, indicating the presence of a significant amount of starting material. In treated material, a C=O stretch at 1705 cm^{-1} is observed. (Note that the C=O stretch of benzoic acid azide is 1680 cm^{-1} due to dimerization.)[32,33] The IR spectrum also reveals a strong absorbance at ca. 1000 cm^{-1}, potentially indicative of the presence of significant amounts of oxidized phosphorus P=O (Figure 11).

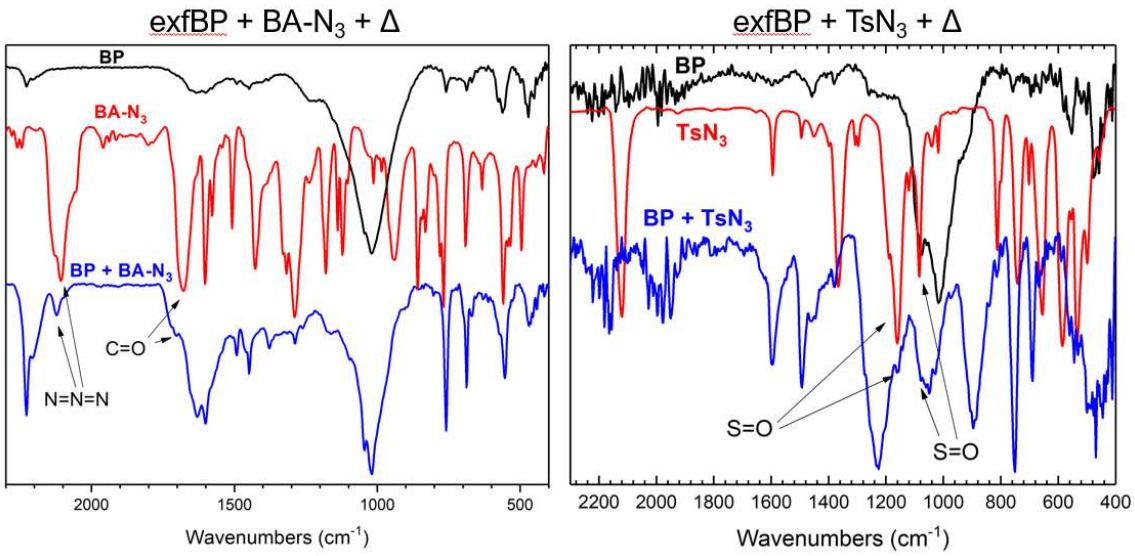

Figure 11. Infrared spectra obtained for *exf*-BP treated with organic azides under moderate (<100 °C) heating.

XPS analysis of benzoic acid azide-treated *exf*-BP reveals an oxidized P component with a high $P_{1,2}$ distance (Figure 12). The area of the oxidized P peak was integrated, revealing ca. 6% of detected phosphorus atoms are oxidized. The binding energy shift is similar to that observed for *exf*-BP oxidized under ambient conditions, corroborating IR evidence of oxidized P *via* P-O or P=O bonds.

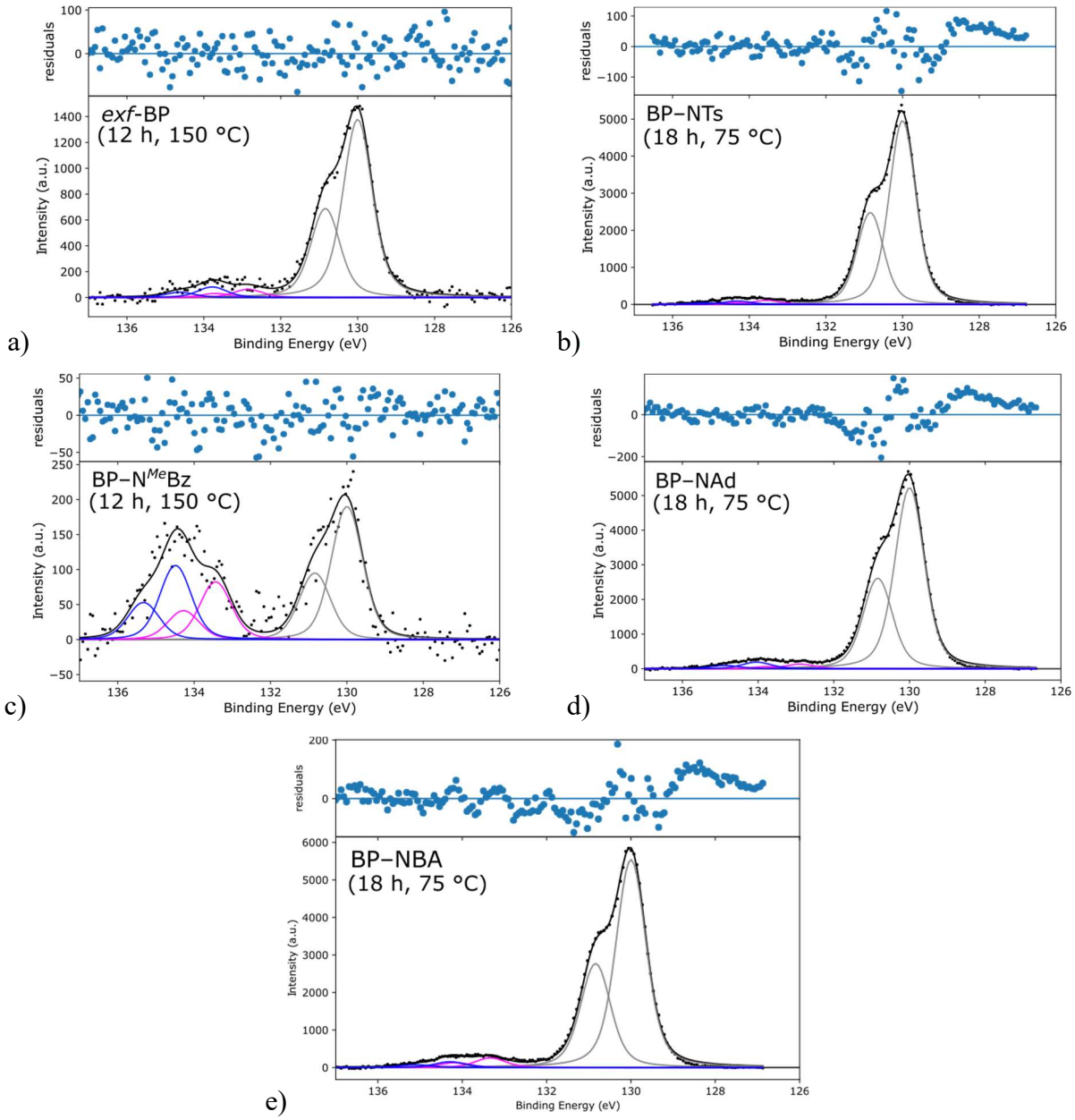

Figure 12. XPS P 2p spectra for thermolytically azide-treated *exf*-BP products. Residual plots for the fits are included above each plot. All P(0) signals were set to 130.0 eV for comparison. The following products are represented: (a) *exf*-BP in benzonitrile heated for 12 h at 150 °C, with roughly 7% of the sampled phosphorus atoms showing oxidation; (b) *exf*-BP heated with TsN_3 in benzonitrile at 75 °C for 18 h; (c) *exf*-BP heated with $^{Me}BzN_3$ in benzonitrile at 150 °C for 12 h; (d) *exf*-BP heated with AdN_3 in benzonitrile at 75 °C for 18 h; (e) *exf*-BP heated with BAN_3 in benzonitrile at 75 °C for 18 h.

3.2 CONCLUSION

Overall, XPS analyses of P 2p core-level spectra consistently show oxidation of BP following treatment with azide precursors under heating. The new P oxidation feature shows a lesser-oxidized character compared to oxidation features arising from ambient oxidation of BP to form P_xO_y species, supporting the formation of P-N or P=N bonds through treatment with azides as opposed to P=O or P-O bonds.

Raman spectroscopy of all thermolyzed azide-treated BP show the 3 characteristic Raman-active modes of BP with no new signals attributed to P-N/P=N groups or Raman-active moieties on the molecular azides. This observation is consistent with none of the azides possessing strong Raman-active vibrational modes, and the Raman inactivity of P-N/P=N bonds.[33] For the BP Raman signals, the ratio of peaks A_g^1/A_g^2 changes to 0.5-0.7 for azide-treated BP under heating, an increase compared to that observed for as-produced exfoliated BP.

Chapter 4. PHOTOLYTIC TREATMENT OF *EXF*-BP WITH ORGANIC AZIDES

General treatment of *exf*-BP under photolytic conditions proceeded through the addition of a slight excess of organic azide to a solution of PhCN under vigorous stirring. The reaction flask was kept sealed under static vacuum throughout the duration of irradiation (2 h) with an Hg vapor lamp, and vigorous stirring was maintained. The nanosheets were then isolated through the same process used in thermolysis reactions, including several washes with organic solvents.

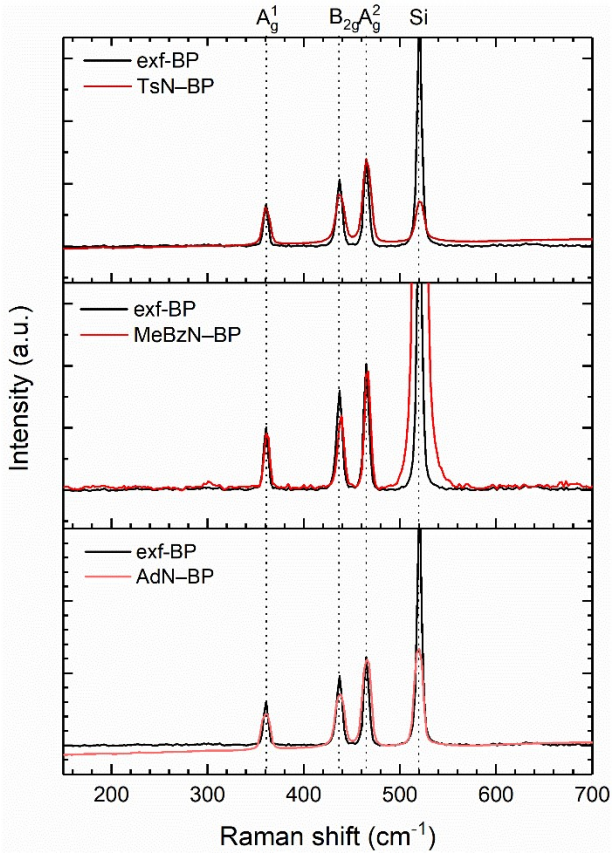

Figure 13. Raman spectrum of untreated *exf*-BP (black) versus exf-BP treated with various azides (shades of red) under photolytic conditions. No other signals are discerned in the full range of 150–3000 cm^{-1}.

Raman spectroscopy reveals light broadening of Raman signals upon treatment, as well as changes in the relative peak ratios of the A_g^1, B_{2g}, and A_g^2 modes (Figure 13). Vibrational

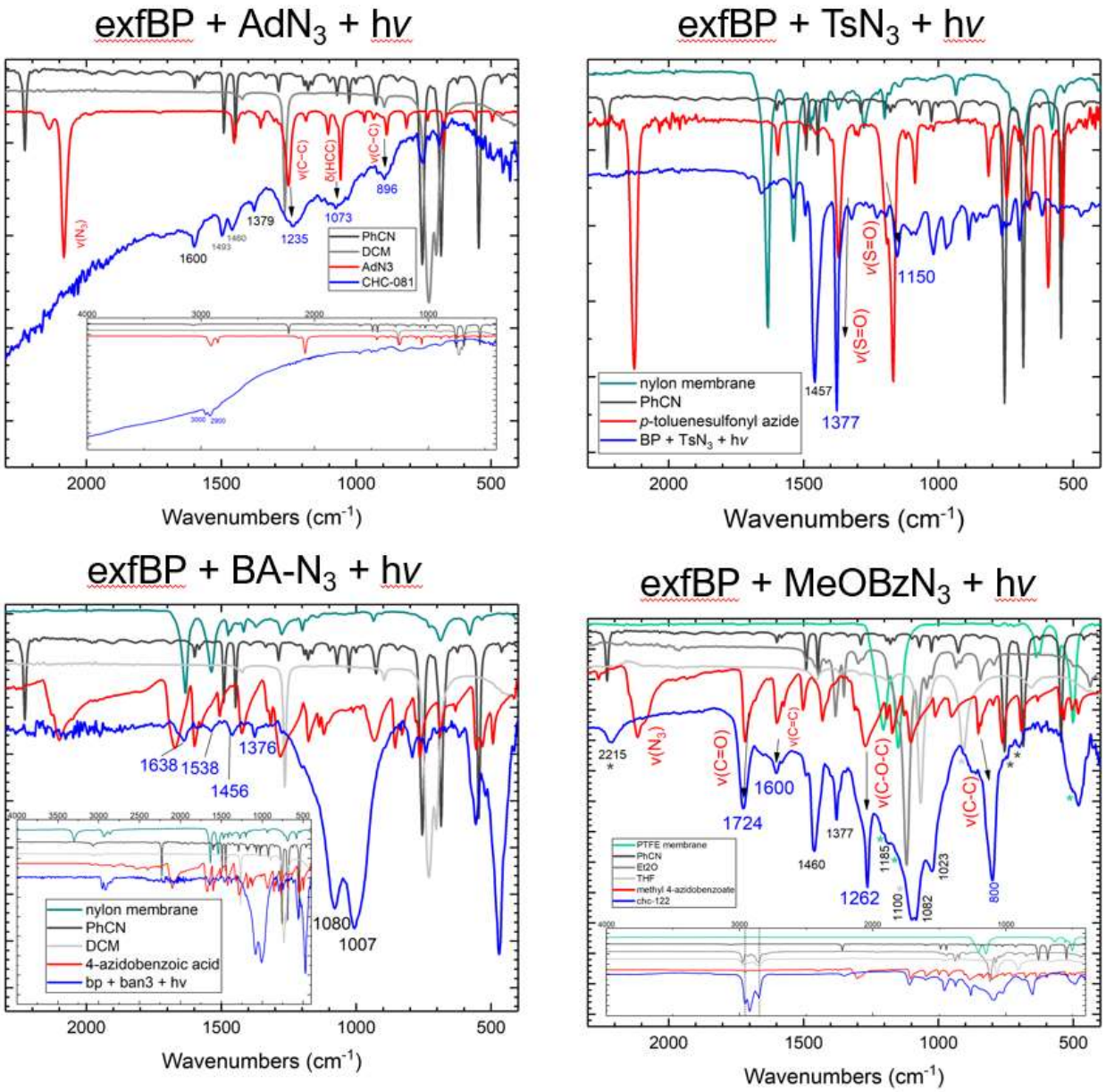

Figure 14. IR spectra of photolytically-treated *exf*-BP using various organic azides.

spectroscopy (DRIFTS, Raman) reveals the presence of sulfonyl S=O and carbonyl C=O stretches in the IR spectra of TsN_3-treated and $MeOBzN_3$-treated *exf*-BP, respectively. The energies of

these bonds are shifted compared to the free, molecular azides. Conclusive assignment of P-N or P=N bonds is complicated by the presence of many signals in the fingerprint region.

The material isolated after the photolysis of adamantyl azide (AdN_3) and BP using the general procedure described above was analyzed using multiple methods, including DRIFTS (IR), XPS, and Raman spectroscopy.

Analysis of a sample of BP in KBr using DRIFTS (IR) spectroscopy reveals the absence of the azide stretch (for AdN_3, $\upsilon_{as}(N_3) = 2083$ cm^{-1}) (Figure 14). In the fingerprint region, three broad absorptions at 1235, 1073, and 896 cm^{-1} are observed corresponding to the υ(C–C), δ(HCC), and υ(C–C) modes of adamantyl azide (1250, 1057, 887 cm^{-1}).

XPS analysis of the sample (P 2p energies) indicates that an oxidized P signal comprising, by area, 7% of the scattered electrons detected from the sample (Figure 15). The intensity of the oxidized P signal is similar to that observed for the heat-treated AdN_3/BP reaction described above. The magnitudes of $P_{1,2}$, however, change slightly, representing an oxidation state of P somewhere between that observed for the heated reaction and P_xO_y. The data is consistent with the formation of P=N bonds on the surface of BP.

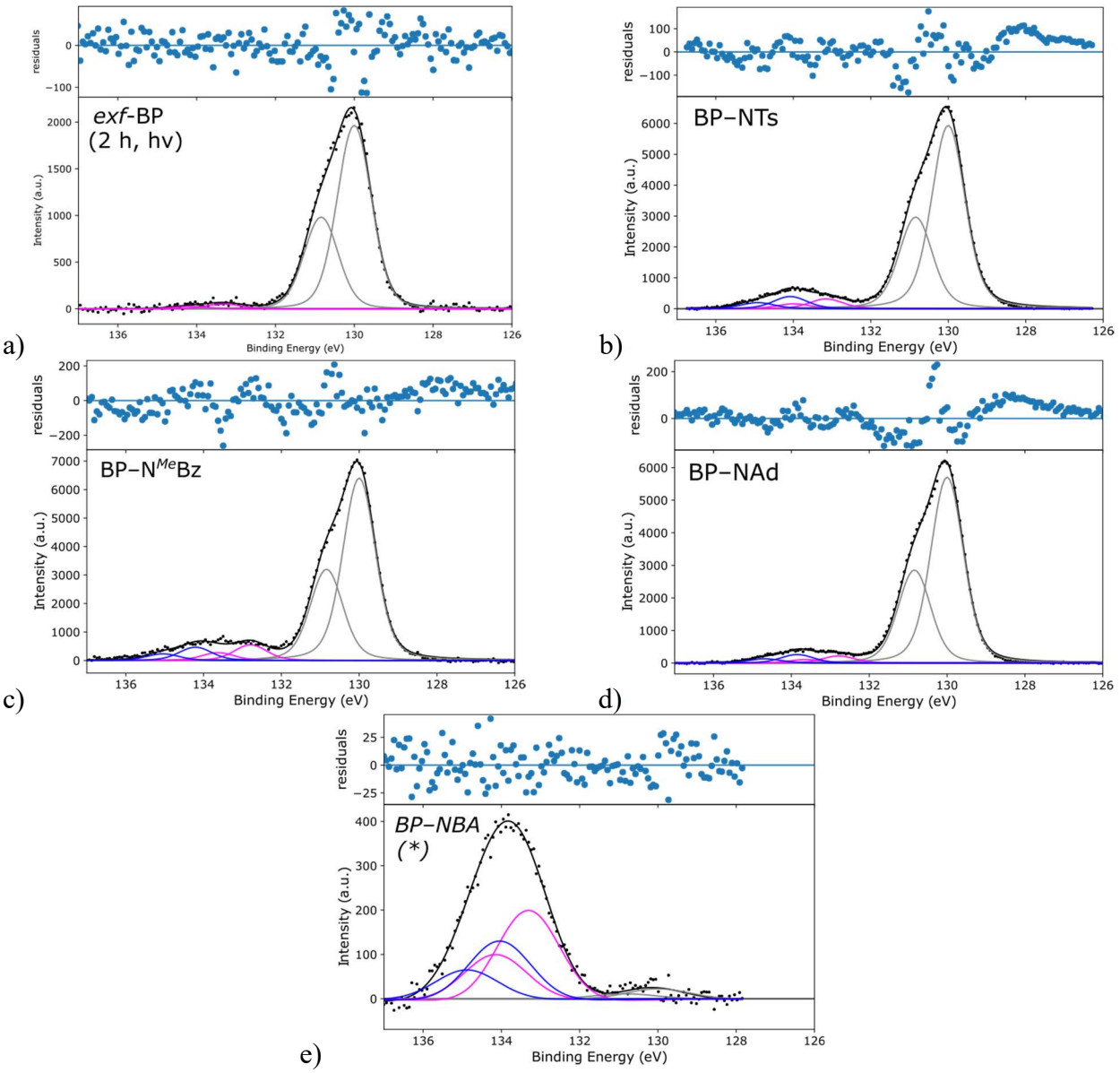

Figure 15. XPS P 2p high-resolution spectra for photolytically azide-treated *exf*-BP products. Residual plots for the fits are included above each plot. All P(0) signals were set to 130.0 eV for comparison. The following products are represented: (a) *exf*-BP irradiated for 2 h, where very little (<3%) signal from oxidized phosphorus atoms is detected from the resultant material; (b) *exf*-BP photo-treated with TsN_3 in benzonitrile for 2 h; (c) *exf*-BP photo-treated with $^{Me}BzN_3$ in benzonitrile for 2 h; (d) *exf*-BP photo-treated with AdN_3 in benzonitrile for 2 h; (e) *exf*-BP photo-treated with BAN_3 in benzonitrile for 2 h, for which the absence of a detectable P(0) signal indicates nearly all detected phosphorus atoms are oxidized. In comparison with *exf*-BP

irradiated in the absence of organic azides, all samples show noticeable levels of chemical activation.

Table 2. Data summary of P 2p XPS data for an assortment of azide treatments using different organic azides. (* = approximate values were obtained due to the near-absence of a detectable P(0) signal. For thermolyzed samples, † = treatments at 75 °C for 18 h, versus ‡ = treatments at 150 °C for 12 h.)

Category	**Sample**	**P_1 Binding Energy (eV)**	**P_2 Binding Energy (eV)**	**(% P_1) / (% P_2)**
Ambient Exposure	*exf*-BP, 2.5 d ambient	3.05	4.23	8% / 8%
Photolyzed	*exf*-BP	-	-	-
	BP–N**Ts**	3.10	4.06	5% / 6%
	BP–N^{Me}**Bz**	2.82	4.22	6% / 7%
	BP–N**Ad**	2.90	3.88	4% / 3%
	BP–N**BA**	3.31*	4.04*	57%* / 37 %*
Thermolyzed	*exf*-BP‡	2.85	3.78	3% / 4%
	BP–N**Ts**†	3.55	4.32	2% / 4%
	BP–N^{Me}**Bz**‡	3.44	4.47	22% / 28%
	BP–N**Ad**†	2.90	4.04	2% / 3%
	BP–N**BA**†	3.34	4.29	4% / 3%

The BP was also analyzed using X-ray emission spectroscopy (XES) to measure its P Kα transition energy (Figure 16). The XES signal indicates that <0.5% of the material is oxidized *via* P=N binding interactions in terms of the total bulk P.

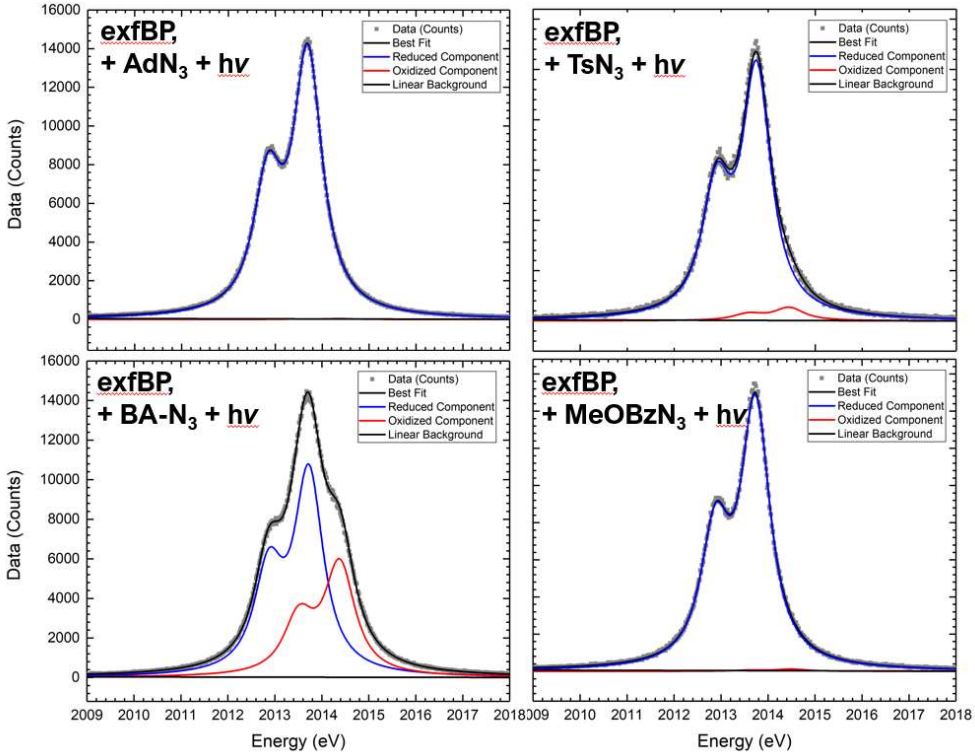

Figure 16. X-ray emission spectra for exfoliated black phosphorus treated with various organic azides under photolytic conditions.

Under photolytic conditions, BP treated with BA-N_3 exhibits a new oxidized XPS P 2p signal (B.E. = 133.4 eV) (Figure 15). However, the unoxidized BP signal entirely disappears, indicating that the entire surface of detected P is oxidized. The P Kα XES signal detects an oxidized component comprising 37% of the total P in the sample, confirming that ca. two-thirds of the total bulk of the sample is unoxidized (Figure 16). The combination of XPS and XES results suggests that BP still comprises the majority of the reaction product, but the unoxidized BP XPS signals are obscured by a thick layer of oxidative byproducts preventing detection through XPS. We note that the extent of oxidation dwarfs that produced through ambient oxidation; thus, introduction of the

benzoic acid azide under irradiation creates a pathway for oxidation even faster than that offered through ambient exposure.

The prevalence of oxidative byproducts is corroborated by DRIFTS. The unreacted azide BA-N_3 has a very strong carbonyl C=O stretching mode at 1690-1705 cm^{-1}, depending on the method of IR analysis (i.e. the extent of hydrogen bonding allowed between -COOH groups). For BP treated with BA-N_3, no C=O signal was observed, indicating consumption of the carboxylic acid moiety (Figure 14). The absence of C=O signals suggests significant degradation of the benzoic acid azide has taken place. We hypothesize 2 concurrent pathways: (1) the formation of a thick, polymeric network consisting of degraded azide byproducts and consumed P, and (2) hydrolysis of P=N bonds with the -COOH group, resulting in the formation of P_xO_y species which further consume BP and are incorporated in the network described in (1).

Qualitatively, significant byproducts from decomposition were observed following photolysis, either alone as a solution in PhCN or as a component in a reaction mixture with BP, especially of BA-N_3 in relation to the other tested azides. These decomposition products have been identified in literature as a mixture of secondary amines and various polymeric products involving the activation of both the carboxylic acid and azide moieties.[32]

To better study BP functionalization with BA-N_3 without the complexities introduced by the reactivity of -COOH, an alternate strategy was pursued through the conversion of the carboxylic acid -COOH into the methyl ester analog -COOMe (or, -$COOCH_3$). The resulting azide, methyl 4-azidobenzoate (herein termed "methyl benzoate azide", or "$MeBzN_3$", for simplicity), was tested in reactions with *exf*-BP. DRIFTS of *exf*-BP treated with $MeBzN_3$ under irradiation confirms the absence of $\upsilon_{as}(N_3)$ = 2114 cm^{-1} following reaction and isolation of the material (Figure 14). Strong new signals are also observed at 1724 (C=O) and 1262 cm^{-1} (C-O-C as.) which closely match the

corresponding groups in free $MeBzN_3$ (υ = 1716 and 1269 cm^{-1}, respectively). Another signal at 1460 cm^{-1} is observed which lies within the range of P=N bonds and bears similarity to a signal observed upon TsN_3 photolysis in the presence of BP. A short further discussion is included on the next page.

The $MeBzN_3$-treated *exf*-BP was also analyzed *via* XES, revealing a P Kα signal with a small contribution from oxidized P (0.9%) (Figure 16). The level of oxidation is significantly smaller than that observed with BA-N_3-treated *exf*-BP, but represents a slight increase in P oxidation versus treatment with AdN_3.

TsN_3 has two characteristic S=O stretching modes at 1380 and 1180 cm^{-1} which are observed in close proximity in DRIFTS analysis of treated BP (Figure 14). A strong new signal also appears in TsN_3-treated BP at 1465 cm^{-1}. The signal falls into the range reported for P=N bonds in literature, 1230-1500 cm^{-1} (s), and bears similarity to the new signal at 1460 cm^{-1} observed in the DRIFT spectrum of $MeBzN_3$-treated BP.[33]

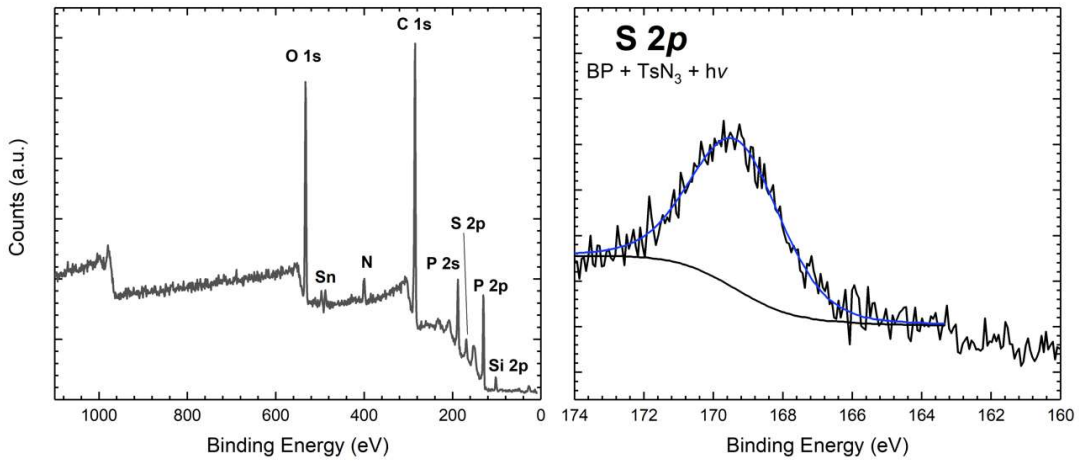

Figure 17. XPS survey spectrum of BP treated with tosyl azide (left), and S 2p core-level spectrum for the same material (right).

After photo-treatment with TsN_3, XPS analysis reveals a significant oxidized P 2p component (13% by area after analysis), with a shift in $P_{1,2}$ values (Figure 15). The XES P Kα signal simultaneously shows 1% oxidation of P throughout the sample (Figure 16).

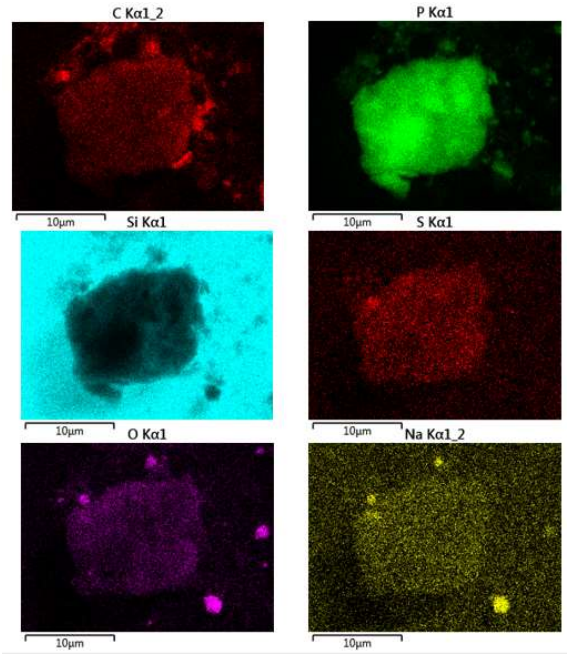

Element	Atomic %
C	20.61
O	0.99
Si	70.57
P	7.81
S	0.02
Total	100.00

Figure 18. SEM images and EDS mapping of the detected elements on BP treated with TsN_3. The Na (and O) Kα signals arise from mild contamination of the sample with zeolites.

A new XPS signal is also detected in the S 2p region which is not observed in the untreated BP (Figure 17). The S 2p signal occurs at 169.3 eV, consistent with signals reported for the sulfur components of tosyl groups and other sulfates/sulfonates. Elemental sulfur is also detected through scanning electron microscopy coupled with energy dispersive X-ray spectroscopy (SEM/EDS), with the detected sulfur well-matched to regions where phosphorus is also detected using EDS mapping (Figure 18). This observation is consistent with the presence of tosyl groups

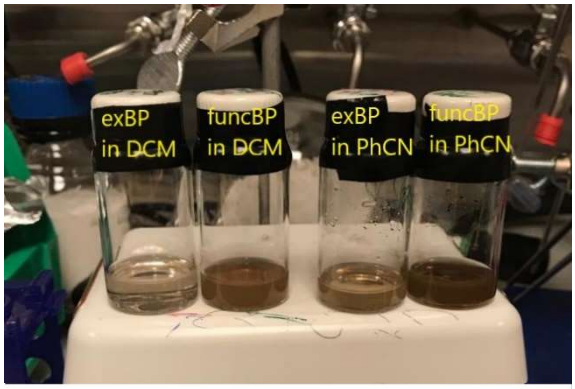

Figure 19. Suspensions of *exf*-BP and TsN_3-treated *exf*-BP in dichloromethane and benzonitrile both show a noticeable increase in dispersibility.

functionalized onto the surface of BP. The total detected proportion of S, when normalized to P, is 0.26%. The SEM/EDS analysis is reasonably consistent with XES data, which detects ca. 1% oxidation of the tosyl-treated *exf*-BP throughout the bulk of the sample.

Qualitatively, the TsN_3-treated *exf*-BP also exhibits increased dispersibility in organic solvents compared with untreated *exf*-BP (Figure 19). This observation matches the expectation of functionalizing the surface of phosphorene with organic moieties, thus increasing its compatibility with organic solvents. An increase in dispersibility is a desirable property, as better-solubilized nanosheets will be less prone to reaggregation over long-term storage in organic solvents.

IR spectra of TsN_3- and BA-N_3-treated BP exhibit new signals consistent with S=O and C=O signals of their molecular analogs, respectively, as well as the absence of $\upsilon_{as}(N_3)$ indicating the consumption of the N_3 moiety. Combined with XPS and XES results distinctively showing oxidation of the BP surface, IR spectra support the successful functionalization of BP with various organic azides under photolytic conditions, putatively through formation of a P=N binding interaction.

Unlike the reactions conducted under mild conditions, the photolyses show $P_{1,2}$ similar to that observed for P_xO_y species. We interpret this result as the formation of a P=N bond through chemical interaction with an organic azide. The similarity in $P_{1,2}$ compared to P_xO_y can be explained by the fact that either (a) P_xO_y species are composed of a mixture of P-O and P=O bonds, and the binding energy shift for P=N should be similar to this average, or (b) the P=N bond has been oxidized to form P=O bonds either during the course of the reaction or before loading the sample into the XPS chamber.

4.1 Determination of the Percent Surface Functionalization Using XPS Results

X-ray photoelectron spectroscopy (XPS) was used to determine the approximate proportion of sampled phosphorus atoms activated *via* covalent interaction, and the extracted proportion was used to evaluate the relative surface coverage of phosphorene with bound organic groups. For XPS analysis, the analysis depth is approximately $3\lambda\sin(\theta)$, where λ is the electron mean free path and θ is the scattering angle measured relative to the plane of the surface. Based on the electron mean free path of black phosphorus ($\lambda \sim 8$ Å), the maximum XPS analysis depth is thus roughly 24 Å, whereas the end-to-end distance between BP layers is approximately 7.4 Å (interlayer spacing + monolayer height = 5.25 Å + 2.1 Å). Thus, the penetration depth achievable through XPS is through less than 3-4 layers of BP. The addition of functional groups to the surface adds further thickness to the material which may render XPS even more selective towards detection of functionalized P versus unexposed P atoms, as the R group functionalities add additional height to the surface (though this additional height may be minimal; calculations reveal that R groups lie parallel to the basal plane in the lowest-energy binding modes of functionalized BP. Beam penetration, as a result, likely limits analysis to the first 2–3 layers of phosphorene. To approximate the surface coverage from covalently-bound nitrene groups, calculations were performed assuming XPS sampling of 2–5 layers of BP.

In this estimation of surface functionalization, we considered that each layer of phosphorene in an *n*-layer thick sheet contains 2*n* distinct sublayers, with only the outer two sublayers accessible for surface treatment. This assumption is illustrated in the diagram below, which represents various thicknesses of analyzed phosphorene. Each layer of phosphorene

presents two surfaces, and unexposed intercalated layers unavailable for functionalization are represented in blue. Exposed surface P atoms are represented in pink.

Note that in this crude estimation we did not include the phosphorus edges, which likely participate in this functionalization process and contribute to the overall percent oxidation of the phosphorus detected using XPS.

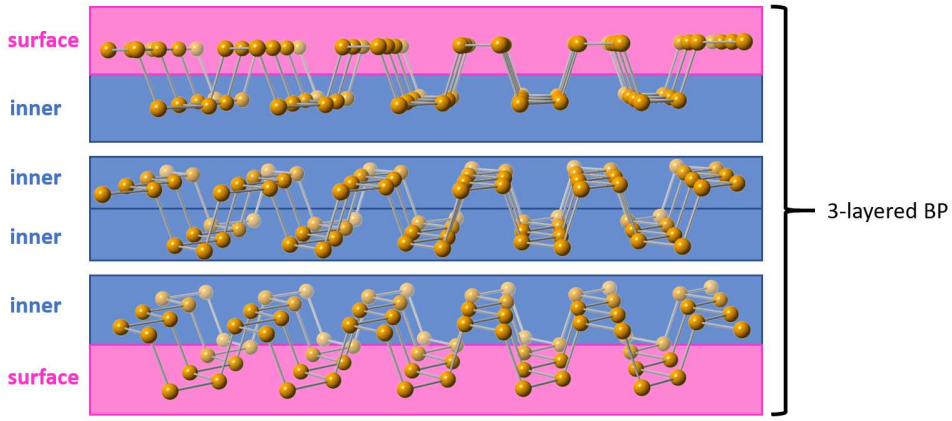

Figure 20. Three-layered *exf*-BP, with the available surfaces for functionalization highlighted in pink. The inner P atoms unavailable for binding are highlighted in blue.

To obtain a rough approximation of the available surface atoms captured in a bond with the nitrene group, the following equation was solved for *x*:

$$\frac{x}{2n} = \left[\text{XPS }\%\left(\text{P}_{1,2}\right)\right]$$

where *x* is the proportion of functionalized surface atoms (in other words, XPS analysis gives the proportion of functionalized surface atoms normalized over the total layers sampled). The factor of 2 assumes that both the top surface and the bottom surface of a sheet are sampled *via* XPS. Assuming the sampling depth limits are from a minimum of 2 layers to a maximum of 3 layers, a range of *x*% surface atoms functionalized can be computed.

Table 3. Approximate percentage of exposed surface atoms activated chemically using various azide functional groups, as determined via XPS and the equations detailed above. TsN_3 and $^{Me}BzN_3$ activation result in similar levels of surface functionalization, whereas AdN_3 activates the surface to a much lower degree.

Sample	XPS %($P_{1,2}$)	*x*% surface functionalization
TsN–BP	11%	44–66%
^{Me}BzN–BP	13%	52–78%
AdN–BP	7%	28–42%

For BA-N_3-treated *exf*-BP, XPS and XES data are consistent with the formation of degradative byproducts forming a thick layer around the *exf*-BP. Treatment with AdN_3, ^{Me}BA-N_3, and TsN_3, assuming a reasonable depth of analysis through 2 layers of *exf*-BP, results in 36%, 64%, and 48% of surface atoms functionalized, respectively.

The parameters $P_{1,2}$ further offers clues about the oxidation state of phosphorus after various transformations with organic azides are performed (Table 2). Apart from BA-N_3, where photolytic byproducts complicate analysis of XPS data, the series of azides tested show a relative trend in the binding energy shift of oxidized P compared to unoxidized P. Thus, the oxidation state of P accessed by thermolytically-oxidized *exf*-BP is lower than that of photolytically-oxidized *exf*-BP. The data suggests that the products of azide treatment under each set of conditions is distinct, and may represent either (a) the formation of a lower-energy bond, such as P–N, under thermolysis versus P=N for photolysis, (b) the reaction proceeds much more slowly under thermolysis compared to photolysis, resulting in lesser surface functionalization which affects $P_{1,2}$, or (c) a combination of both (a) and (b).

4.1.1 *Layer Thickness Determination via Comparative Analysis of XPS and XES*

X-ray emission spectroscopy (XES) enables detection of X-ray emission throughout the bulk of the sample and is not restricted by beam penetration depth like XPS. To compare XPS and XES results, the following equation was used to calculate the approximate number of layers in a sheet of functionalized BP based on the percentage of functionalized BP determined through XES P Kα analysis as well as the percentage of functionalized surface P atoms obtained from the previous analysis. The following equation was solved for *n*:

$$\frac{x}{N} = [\text{XES } \%(\text{P}_{\text{oxid}})]$$

where *x* is the proportion of functionalized surface atoms obtained from the previous section's calculations, and *N* is the total number of phosphorene layers in the analyzed flake. The equation assumes a simple distribution of BP sizes allowing for approximation of the mean thickness *N*.

Sample	***x*% surface functionalization**	**XES %(P_{funct})**	**Calculated *N***
TsN–BP	44 - 66%	5.2%	9 - 13
^{Me}BzN–BP	52 - 78%	0.9%	58 - 87
AdN–BP	28 - 42%	0.3%	93 - 140

4.2 TESTING THE AMBIENT STABILITY OF RN–BP (R = TS, ^{ME}BZ, AD) USING UV-VIS AND XPS

4.2.1 *Measuring the Ambient Stability of TsN–BP with XPS*

A suspension of TsN–BP (produced in Section 5.2.2.4 using *Workup C*) was concentrated *in vacuo* and drop-cast onto an Au-coated Si substrate. Several substrates were prepared in parallel from an identical stock solution of combined TsN–BP batches. The substrates were stored in a N_2 glovebox and sequentially removed from the glovebox and exposed to ambient conditions of light and humidity for the specified amount of time (1–5 days). The samples were subsequently analyzed *via* XPS.

4.2.2 *Measuring the Ambient Stability of RN–BP (R = Ts, ^{Me}Bz, Ad) with UV–Vis Spectroscopy*

To prepare RN–BP materials, the procedure in Section 5.2.2.4 was followed and *Workup C* was slightly modified: after the final wash step, the solids collected on the PTFE membrane were transferred to separate vials and resuspended in 5 mL milli-Q water under ambient conditions using ultrasonication. Two controls were prepared: (1) untreated *exf*-BP in PhCN, and (2) photo-treated *exf*-BP following the treatment described in Section 5.2.2.4.

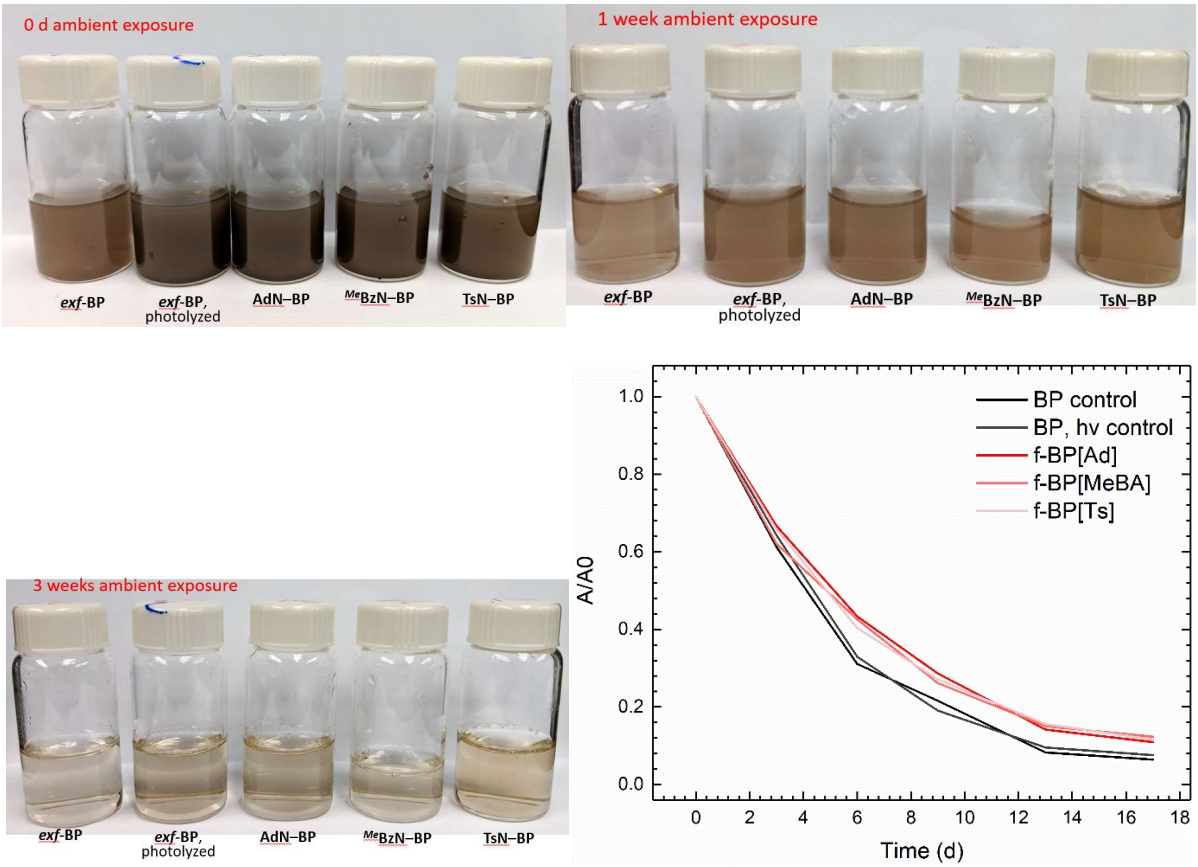

Figure 21. Images of various *exf*-BP and RN–BP suspensions stored in oxygen-containing milli-Q H_2O under ambient conditions for 0 days, 1 week, and 3 weeks. The eventual disappearance of BP's distinctive brown color, which is associated with the degradative oxidation of brown BP into colorless H_3PO_4 and P_xO_y species, was measured using UV–vis spectroscopy (bottom right). Time evolution UV–vis spectra corresponding aqueous solutions of functionalized BP (RN-BP, R = Ts, ^{Me}Bz, Ad) and control samples (*exf*-BP and photolyzed *exf*-BP).

All suspensions were stored in air and measured once every 3-4 days for a total of 6 timepoints spanning 17 days. The absorption spectrum of a cuvette filled with milli-Q water was subtracted from the spectra acquired for each sample. All spectra baselines were fixed to zero. To calculate the decay in absorbance over time, the absorbance of each suspension (A) at 460 nm was measured and normalized to the t = 0 d absorbance (A_0) in accordance with a previous protocol.[34]

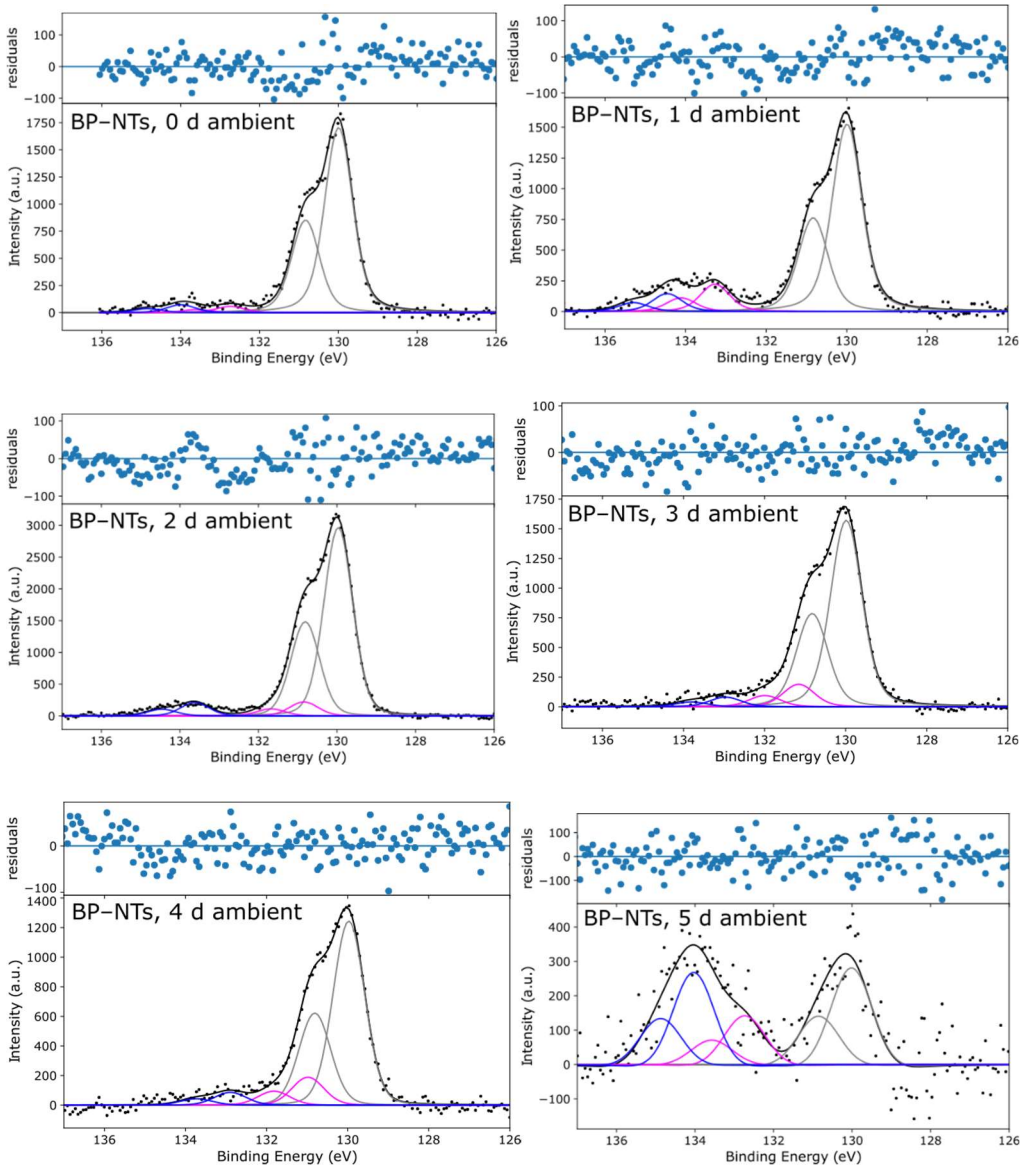

Figure 22. Time-resolved data for BP–NTs samples exposed to ambient conditions from 0 to 5 d.

4.3 CONCLUSION

The photolytic treatment of *exf*-BP with organic azides was demonstrated; significant reduction in reaction time was achieved *versus* thermolytic treatment (including thermolytic literature protocols). Covalently functionalized *exf*-BP was characterized extensively using vibrational spectroscopy, X-ray analyses, and microscopy. Using XPS, surface activation was approximated at *ca.* 30-80%.

In results not discussed in this work, infrared spectroscopy with isotopic (^{15}N) labeling was used to identify P=N signals in the functionalized material, representing the first known rigorous identification of a P=N signal in the literature. We hope this work will lend precedence towards similar rigor in other covalently modified BP systems.

The ambient stability of the material does not show significant enhancement over untreated *exf*-BP. Further work to probe the mechanism for hydrolysis of the P=N bond, and potential access to a stable intermediate phosphorene oxide, is planned.

Chapter 5. EXPERIMENTAL METHODS

5.1 General Considerations

Unless stated otherwise, all work was performed under an inert atmosphere of N_2 using a Schlenk line and associated techniques, or inside of an LC Technology Solutions, Inc. glove box containing <5 ppm H_2O and O_2. Anhydrous solvents were obtained from a SciMatCo solvent system and stored over 3 Å molecular sieves (Thermo-Fisher) for at least 12 h before use. The molecular sieves were previously activated by heating at 250 °C, under vacuum (<50 mTorr) for at least 3 days. All water used in experimentation was deionized; ultra-pure milli-Q water with a resistivity of >18 MΩ·cm was used instead when specified. Black phosphorus (BP) crystals (99.998%, Smart Elements) were purchased and used as received. Benzonitrile (99%, Alfa Aesar) was degassed for several hours under vacuum and stored over sieves for a minimum of 2 days prior to use. All glassware was dried overnight at 150 °C prior to use. Centrifugation, unless otherwise stated, was performed by transferring suspensions into Nalgene™ Oak Ridge High-Speed Centrifuge Tubes (made of PTFE FEP, for superior solvent resistance). Centrifuge tubes were sealed with O-ring caps to prevent ambient exposure. Sonication was performed using a 110W bath sonicator at 40 kHz that was maintained at 22−28 °C under circulation cooling. Filtrations were performed using EMD Millipore Omnipore membrane filters, with a pore size of 0.2 μm.

All azides were stored in the dark in the glovebox freezer (−35 °C) and thawed at room temperature prior to use. NaN_3 (>99.5%, Sigma-Aldrich), $Na^{15}N^{14}N_2$ (>98%, Cambridge Isotope Laboratories), 1-azidoadamantane (AdN_3, 97%, Sigma-Aldrich), and methyl 4-aminobenzoate (98%, Aldrich) were used as received from the supplier. Concentrated hydrochloric acid (HCl, 36.5-38.0%, ACS grade, Macron Fine Chemicals) was diluted with deionized or milli-Q water to

specified concentrations. Sulfuric acid (H_2SO_4, 36 N, ACS grade, Fisher Scientific) was used as-received without further dilution. Prior to use, 4-azidobenzoic acid (BAN_3, 97%, TCI America) was redissolved in diethyl ether, the resulting solution was filtered to remove solid impurities, and the filtrate collected and brought to constant mass *in vacuo*.

Photolytic treatments were performed *via* irradiation from a 450 W medium-pressure mercury vapor lamp (Hanovia Specialty Lighting, PC 451.050) emitting 200–400 nm broadband radiation. The lamp was hosted inside a quartz jacket that was continuously cooled with tap water to maintain the reactions at ambient temperature. Quartz reaction flasks were purchased from Aldrich.

For spectroscopic analysis, test-grade Si wafers (University Wafer) and Au-coated Si wafers (100 nm Au, Platypus Technologies) were cut, rigorously washed by sequential sonication with detergent (Si only), water (Si only), acetone, and isopropanol, and then oven-dried overnight at 150 °C prior to use.

NMR spectra were obtained on a Bruker AVance 300 spectrometer and analyzed using Bruker's TopSpin software package. Attenuated total reflectance infrared (ATR-IR) spectra were recorded on a Bruker Alpha IR instrument equipped with a Platinum ATR accessory. Diffuse reflectance infrared Fourier transform spectroscopy (DRIFTS) was used in some analyses with the corresponding Bruker DRIFTS accessory, in conjunction with an agate mortar and pestle, and FT-IR grade potassium bromide (KBr, >99%; Alfa Aesar). Raman spectra were acquired on a Renishaw InVia microscope using a 514 nm Ar laser and a 50× microscope objective. UV–vis–NIR spectra were acquired using a Varian Cary 5000 UV–vis–NIR double-beam spectrophotometer. XRD spectra were acquired on a Bruker D8 Discover powder X-ray diffractometer with a large-area Pilatus 100K large-area 2D detector. Scanning electron

microscope images were obtained on an FEI Sirion XL30 Scanning Electron Microscope (SEM) integrated with an Oxford Instruments Energy Dispersive X-ray Spectrometer (EDS). XPS/ESCA analysis was performed on a Surface Science Instruments (SSI) S-Probe system under ultrahigh vacuum. AFM images were measured in non-contact mode on an Asylum Research Cypher atomic force microscope under a flow of N_2. All images were acquired using electrically conductive Cr/Pt AFM probes.

5.1.1 *General Information for XPS, XES, Powder-XRD, and Raman Spectroscopy: Sample Preparation and Analysis*

To prepare samples for spectroscopic analyses, suspensions of various phosphorene products in dichloromethane or tetrahydrofuran were drop-cast onto clean wafers and then annealed for 2-5 min at 80 °C before analysis.

In certain XPS analyses, Si loss peaks interfered with S 2p signals. Thus, XPS analyses were also conducted using identical preparations, but using Au-coated Si wafers. Samples measured using traditional Si substrates are indicated.

5.1.2 *X-Ray Photoelectron Spectroscopy (XPS) Data Analysis Details*

Rough analysis of survey spectra was performed using Esca Hawk7 software. Binding energies were referenced to adventitious carbon (B.E.[C 1s] = 285.0 eV). All P 2p spectra were analyzed using linear combination fitting with the nonlinear least-squares fitting Python package LMFIT.[30] Shirley baselines were subtracted from spectra prior to analysis. Paired pseudo-Voigt profiles representing the (P $2p_{3/2}$, P $2p_{1/2}$) doublet were fit to baseline-subtracted data, with a fixed peak separation of 0.84 eV and relative ratio of 2:1, consistent with reported values for phosphorus.[35] The Gaussian width To fit multiple P peak shapes, widths of subsequent signals were constrained

to the width of the (P $2p_{3/2}$, P $2p_{1/2}$) pair. Relative contributions of each unique peak shape were measured according to the relative intensity of the signal. The center of the P $2p_{3/2}$ signal was fixed to 130.0 eV for comparative analysis.

5.1.3 *X-Ray Emission Spectroscopy (XES) Details*

Phosphorus Kα XES measurements were performed using a recently developed laboratory spectrometer, described in detail by Holden *et al*.[36] The spectrometer uses a low-power, 50 Watt Pd-anode X-ray tube (Varex) to stimulate fluorescence in the sample. The fluorescence is analyzed in the Dispersive Refocusing Rowland (DRR) geometry using a 10 cm-radius of curvature, cylindrically bent, Si (111) Johann crystal analyzer (XRSTech). The analyzed rays are detected using an energy-resolving CMOS-based color X-ray camera.[37] The spectrometer is contained in a vacuum chamber which is evacuated to a pressure of <100 mTorr during measurements to reduce air absorption. The phosphorene samples were prepared for XES measurements by drop-casting onto silicon wafers with an approximate sample spot area of ~3–4 mm in diameter. The prepared samples were kept under inert atmosphere, and briefly exposed to air (<5 minutes) during loading into the spectrometer.

5.2 SYNTHETIC PROTOCOLS

5.2.1 *Starting Materials*

5.2.1.1 Synthesis of *p*-Toluenesulfonyl Azide (TsN_3, Ts = *p*-$CH_3(C_6H_4)SO_2$)

In a modified literature protocol,[38] a colorless slurry of sodium azide (NaN_3; 1.95 g, 30 mmol, 1.5 equiv) in anhydrous acetone (20 mL; HPLC grade, Fisher Scientific) was added a solution of *p*-toluenesulfonyl chloride (TsCl; 3.81 g, 20 mmol, 1 equiv) in anhydrous acetone (20 mL). The flask was covered with aluminum foil to protect against light exposure, and vigorously stirred for

22 h to yield a slightly yellow slurry. The solids were separated by filtration through a pad of Celite and the reaction solution was rotoevaporated to produce a light yellow oil. This oil was placed under vacuum (<50 mTorr) to yield the spectroscopically pure *p*-toluenesulfonyl azide (3.02 g, 15.3 mmol, 77%). ^{1}H NMR ($CDCl_3$, 300 MHz) δ: 7.85 (d, 2 H), 7.40 (d, 2 H), 2.48 (s, 2 H) ppm. IR (ATR): $\nu_{asym}(N_3)$ = 2120 cm^{-1}.

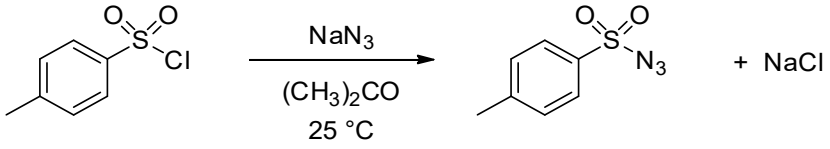

5.2.1.2 Synthesis of p-Toluenesulfonyl Azide, 15N-Labeled (TsN215N/Ts15NN2)

$$\text{Ts-Cl} + \text{Na}[^{15}\text{NNN}] \rightarrow 0.5\ \text{Ts-}^{15}\text{NNN} + 0.5\ \text{Ts-NN}^{15}\text{N} + \text{NaCl}$$

A similar procedure was used to synthesize the ^{15}N-labeled tosyl azide from terminally-labeled sodium azide. To a 50-mL pear shaped flask containing a solution of $Na^{15}NN_2$ (135 mg, 2.05 mmol, 1.02 equiv) in water (1 mL), TsCl (381 mg, 2.0 mmol, 1 equiv) was added as a solution in anhydrous acetone (5 mL). The flask was covered with aluminum foil and the solution was stirred for 16 h at room temperature. Acetone was removed *in vacuo*, and the resulting residue was washed with dichloromethane (DCM; 3 mL) and water (1 mL). The aqueous extracts were washed again with DCM (2 mL) and the organic extracts were combined and dried over anhydrous Na_2SO_4. The volatiles in the filtrate were removed under vacuum to afford the product as a white powder (360 mg, 1.82 mmol, 90% yield). IR (ATR): $\nu_{asym}(N_2{}^{15}N)$ = 2102, 2122 cm^{-1}.

5.2.1.3 Synthesis of Methyl 4-Azidobenzoate ($^{Me}BzN_3$)

In a protocol adapted from literature,[39] 4-azidobenzoic acid (1.49 g, 9.13 mmol) was dissolved in methanol (45 mL; Sigma Aldrich, HPLC grade) to form a yellow-orange solution to which 15

drops of H_2SO_4 were subsequently added. The mixture was heated to 65 °C for 25 h, and the volatile materials were removed *in vacuo* to yield a light orange solid. The solids were redissolved in a small amount of DCM (*ca.* 15 mL) and washed sequentially with saturated aqueous $NaHCO_3$ (30 mL H_2O), DCM (3×50 mL), and NaCl brine (2×40 mL). The product was dried over $MgSO_4$, filtered, and then placed under vacuum for *ca.* 6 h, yielding methyl 4-azidobenzoate as a spectroscopically pure, light orange solid (1.35 g, 83% yield). ^{1}H NMR ($CDCl_3$, 300 MHz) δ: 3.91 (s, 3 H), 7.07 (d, 2 H), 8.04 (d, 2 H). IR (ATR): $\nu_{asym}(N_3)$ = 2114 cm^{-1}, ν(C=O) = 1716 cm^{-1}.

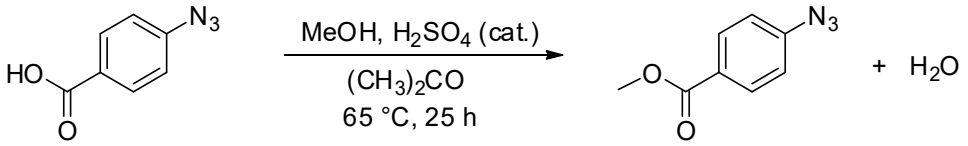

5.2.1.4 Synthesis of Methyl 4-Azidobenzoate, ^{15}N-Labeled ($^{Me}Bz^{15}NN_2$/$^{Me}BzN_2{}^{15}N$)

In a protocol adapted from literature,[40] methyl 4-aminobenzoate (171 mg, 1.13 mmol, 1 equiv) was loaded into a 25-mL pear-shaped flask, and dissolved in diluted HCl (0.2 M, 5 mL). Extra water (2 mL) was added to aid dissolution, and the flask was sealed with a rubber septum. After cooling to 0 °C, $NaNO_2$ (79 mg, 1.14 mmol, 1.01 equiv) was dissolved in deionized water (2 mL) and added dropwise *via* a syringe to the benzoate solution. $Na^{15}NN_2$ (75 mg, 1.14 mmol, 1.01 equiv) in water (1 mL) was then added dropwise *via* syringe, and the mixture was diluted with 9 mL water. After 30 mins of stirring, the mixture was removed from the bath and allowed to warm to room temperature. The crude reaction mixture was washed with Et_2O (2 × 10 mL) and water (1×10 mL), then dried over anhydrous Na_2SO_4, filtered, and placed under vacuum. The resulting light beige powder was redissolved in Et_2O (10 mL), filtered through a plug of anhydrous silica gel, and then dried under vacuum to yield spectroscopically pure product (156 mg, 0.88 mmol, 78%). IR (ATR): $\nu_{asym}(N_2{}^{15}N)$ = 2070, 2118 cm^{-1}, ν(C=O) = 1718 cm^{-1}.

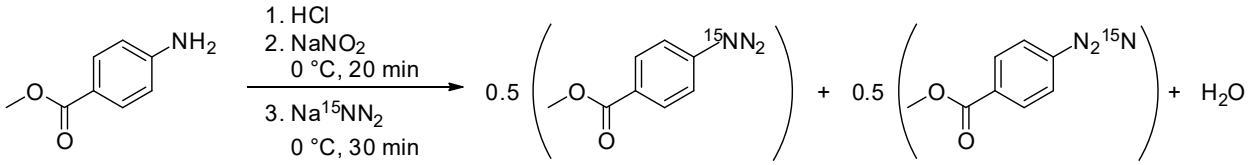

5.2.1.5 Synthesis of Exfoliated Black Phosphorus Nanosheets (*exf*-BP)

Crystals of black phosphorus (BP; 60 mg) were finely crushed in an agate mortar and pestle. The resulting fine, silver-black powder was subsequently sonicated in the dark for 20 h in anhydrous benzonitrile (120 mL). Air-free 250-mL Schlenk flasks sealed with Teflon stoppers were used to contain the solution to prevent air exposure. The resulting suspensions were brown and opaque.

Figure 23. *exf*-BP in PhCN produced from the *standard workup* (left) *vs*. *exf*-BP in PhCN produced from the *modified workup* (right). Note the clarity of the solution produced from the *standard workup* in contrast to the "cloudy" or semi-opaque suspension produced from the *modified workup.*

The ***standard workup*** includes as a first step the removal of larger, unexfoliated sediments, *via* centrifugation for 1 h at 2000*g* (units equivalent to relative centrifugal force, rcf). The yellow-brown supernatants containing *exf*-BP solutions (Figure 23, left) were stored and consumed within 2 days of preparation.

A ***modified workup*** was used for the material produced in Sections 5.2.2.1 (with AdN_3 and TsN_3 only; page 53) and 5.2.2.4 (with $^{Me}BzN_3$ and AdN_3 only; page 54) was centrifuged at 500*g* instead

of 2000*g*, in order to afford isolation of a larger amount of product (Figure 23, right). The effects of the modified workup will be discussed later in subsequent surface analysis sections.

5.2.2 *Functionalization of exf-BP with Organic Azides*

All reactant stoichiometries were based on an approximated concentration of *exf*-BP nanosheets in benzonitrile. The concentration was estimated using UV-vis extinction coefficients reported previously.[28] An average calculated concentration of 1.67±0.75 mM was obtained from measuring 15 different batches of *exf*-BP solutions, each prepared using the *standard workup* method described above in 2.1.5. Molar equivalencies were calculated relative to all phosphorus atoms present in solution (*i.e.* excess of azide was used relative to the surface phosphorus atoms available for reactivity). During photolysis, reaction mixtures were stirred vigorously in Pyrex flasks, which were clamped at a distance of <10 cm from the light source.

5.2.2.1 Thermolytic Treatment of *exf*-BP with AdN_3, TsN_3 and 4-Azidobenzoic Acid (BAN_3)

exf-BP solution (50 mL, 1 equiv, 1.67 mM) and the organic azide (0.33 mmol, 3.99 equiv) were added to a scintillation vial equipped with a Teflon stirbar. The vial was sealed with thermoset caps lined with PTFE, and heated for 18 h in an aluminum heating block set to 75 °C. The resulting suspension was centrifuged at 24,600*g* for 2 h at 4 °C, and the supernatant was carefully removed. The remaining solids were transferred to a 1.5-mL polypropylene Eppendorf tube and resuspended in tetrahydrofuran (THF, *ca.* 1.2 mL) using a sonicator. The solids were washed with THF (3×1.2 mL), then DCM (1×1.2 mL), and finally resuspended in *ca.* 0.5 mL DCM for sample preparation (*via* drop-casting).

5.2.2.2 Thermolytic Treatment of *exf*-BP with $^{Me}BzN_3$

Inside the glovebox, a 50 mL Schlenk tube equipped with a Teflon stirbar was charged with a solution of *exf*-BP (30 mL, 1.67 mM, 1 equiv) and methyl 4-azidobenzoate (35 mg, 0.20 mmol, 3.99 equiv). The reaction mixture was connected to a nitrogen-filled Schlenk line and opened to an oil bubbler, and under vigorous stirring, was heated to 150 °C for 12 h. The flask was brought back inside the glovebox, and the solids were isolated on a 0.2 μm PTFE filter membrane, then washed with PhCN (1×30 mL) and THF (1×30 mL). The solids were resuspended in THF (*ca.* 5-10 mL). Prior to analysis, the volatiles we removed under reduced pressure.

5.2.2.3 Control: Thermolysis of *exf*-BP

A Schlenk flask equipped with a Teflon stirbar was loaded with a solution of *exf*-BP (30 mL, 1.67 mM, 1 equiv). The flask was vigorously stirred at 150 °C for 12 h under a low flow of N_2 gas on a Schlenk line. No color change or other visual indicators differentiated the resulting mixture from the original *exf*-BP solution. In a glovebox, the reaction mixture was filtered through 0.2 μm PTFE filter membranes to isolate the solid product, which was washed sequentially with PhCN (1×30 mL) and THF (1×30 mL). The solids were redispersed in THF (*ca*. 5-10 mL), and the volatiles removed *in vacuo* prior to further analysis.

5.2.2.4 Photolytic Treatment of *exf*-BP with Organic Azides

exf-BP (30 mL, 1.67 mM in PhCN, 1 equiv) and the organic azide (BAN_3, AdN_3, TsN_3, $^{Me}BzN_3$, $Ts^{14/15}NN^{14/15}N$ or $^{Me}Bz^{14/15}NN^{14/15}N$, respectively; 0.20 mmol, 4.0 equiv) were loaded into a Schlenk flask equipped with Teflon-coated stirbars. Prior to photolysis, the headspace of the flask was evacuated to accommodate the N_2 evolved during the reaction. The reaction mixture was irradiated for 2 h under vigorous stirring.

The resulting reaction mixture was passed through a 0.2 μm PTFE membrane. Three different workup procedures (*A*, *B* and *C*, detailed below) were explored for purifying the treated nanosheets, and isolating them off the PTFE membranes.

Workup A: the collected solids were washed on the membrane with DCM (5×2 mL) and resuspended in DCM (*ca.* 5 mL) for storage.

Workup B: the collected solids were washed on the membrane with N,N-dimethylformamide (DMF, 5×2 mL), followed by PhCN (5×2 mL), and then by DCM (5×2 mL). Finally, the material was resuspended in DCM (*ca.* 5 mL) for storage. *This workup was used only with BAN_3-treated exf-BP filtered through PTFE membranes, under both thermolytic and photolytic conditions (Sections 5.2.2.1 and 5.2.2.4).*

Workup C: the collected solids were washed on the membrane with PhCN (1×30 mL) and then THF (1×30 mL) before the solids were resuspended in THF (ca. 5 mL) for storage. This workup was used to isolate the majority treated materials, including most azide treatments (with the exception of BAN_3) and products of all ^{15}N labeling experiments.

5.2.2.5 Photolytic Treatment of *exf*-BP with Extra Equivalents of TsN_3 Added After 1 h Irradiation

To a 50 mL Schlenk flask equipped with a Teflon stirbar, *exf*-BP (30 mL, 1.67 mM, 1 equiv) and tosyl azide (39 mg, 0.20 mmol, 4.0 equiv) were added. The headspace of the flask was evacuated, and the flask and its contents were subjected to UV irradiation under vigorous stirring. After 1 h, the flask was removed from the light source and another four equivalents of tosyl azide (39 mg, 0.20 mmol, 4.0 equiv) were added. The flask was then returned to the lamp for an additional 1 h of irradiation. During this time the reaction mixture took on a red-orange color. The resulting material was isolated using *Workup C*, described in Section 2.2.4.

5.2.2.6 Photolytic Treatment of *exf*-BP in a Quartz Flask

A 100 mL quartz round bottom flask equipped with a Schlenk air-free adapter and a Teflon stirbar, was loaded with a solution of *exf*-BP (30 mL, 1.67 mM, 1 equiv), and tosyl azide (39 mg, 0.20 mmol, 4.0 equiv), and its headspace was evacuated. The flask was irradiated for 2 h, when the solution took a wine-red color. The dark brown product was isolated using *Workup C*, described in Section 2.2.4.

5.2.2.7 Control: Photolysis of *exf*-BP

A 50 mL Schlenk tube equipped with a Teflon stirbar was loaded with *exf*-BP (30 mL, 1.67 mM, 1 equiv) and sealed with a Teflon stopper. The headspace of the flask was evacuated, and the flask was irradiated for 2 h under vigorous stirring. No color change or other visual cues were observed in the photo-treated solution. The brown solids were isolated using *Workup C*, described in Section 2.2.4.

BIBLIOGRAPHY

[1] G. Bottari, M. Ángeles Herranz, L. Wibmer, M. Volland, L. Rodríguez-Pérez, D. M. Guldi, A. Hirsch, N. Martín, F. D'Souza, T. Torres, *Chem. Soc. Rev.* **2017**, *46*, 4464.

[2] V. Tran, R. Soklaski, Y. Liang, L. Yang, *Phys. Rev. B* **2014**, *89*, 235319.

[3] H. Liu, A. T. Neal, Z. Zhu, Z. Luo, X. Xu, D. Tománek, P. D. Ye, *ACS Nano* **2014**, *8*, 4033.

[4] L. Li, Y. Yu, G. J. Ye, Q. Ge, X. Ou, H. Wu, D. Feng, X. H. Chen, Y. Zhang, *Nat. Nanotechnol.* **2014**, *9*, 372.

[5] X. Ling, H. Wang, S. Huang, F. Xia, M. S. Dresselhaus, *Proc. Natl. Acad. Sci.* **2015**, *112*, 4523.

[6] S. Das, W. Zhang, M. Demarteau, A. Hoffmann, M. Dubey, A. Roelofs, *Nano Lett.* **2014**, *14*, 5733.

[7] J. Qiao, X. Kong, Z. Hu, F. Yang, W. Ji, *Nat. Commun.* **2014**, *5*, 4475.

[8] F. Xia, H. Wang, Y. Jia, *Nat. Commun.* **2014**, *5*, 1.

[9] J. Guan, Z. Zhu, D. Tománek, *Phys. Rev. Lett.* **2014**, *113*, 1.

[10] Y. Wang, B. Yang, B. Wan, X. Xi, Z. Zeng, E. Liu, G. Wu, Z. Liu, W. Wang, *2D Mater.* **2016**, *3*, 035025.

[11] A. Ziletti, A. Carvalho, D. K. Campbell, D. F. Coker, A. H. Castro Neto, *Phys. Rev. Lett.* **2015**, *114*, 26.

[12] X. Niu, Y. Li, Y. Zhang, Q. Li, Q. Zhou, J. Zhao, J. Wang, *J. Phys. Chem. Lett.* **2018**,

5034.

[13] A. Favron, E. Gaufrès, F. Fossard, A.-L. Phaneuf-L'Heureux, N. Y. W. Tang, P. L. Lévesque, A. Loiseau, R. Leonelli, S. Francoeur, R. Martel, *Nat. Mater.* **2015**, *14*, 826.

[14] C. R. Ryder, J. D. Wood, S. A. Wells, Y. Yang, D. Jariwala, T. J. Marks, G. C. Schatz, M. C. Hersam, *Nat. Chem.* **2016**, *8*, 597.

[15] M. van Druenen, F. Davitt, T. Collins, C. Glynn, C. O'Dwyer, J. D. Holmes, G. Collins, *Chem. Mater.* **2018**, *30*, 4667.

[16] H. Staudinger, J. Meyer, *Helv. Chim. Acta* **1919**, *2*, 635.

[17] P. Molina, C. López-Leonardo, J. Llamas-Botía, C. Foces-Foces, C. Fernández-Castaño, *Tetrahedron* **1996**, *52*, 9629.

[18] M. Alajarín, P. Molina, A. López-Lázaro, C. Foces-Foces, *Angew. Chemie* **1997**, *109*, 147.

[19] X. Liu, N. Thirupathi, I. A. Guzei, J. G. Verkade, *Inorg. Chem.* **2004**, *43*, 7431.

[20] R. D. Kennedy, *Chem. Commun.* **2010**, *46*, 4782.

[21] T. Meguro, S. Yoshida, K. Igawa, K. Tomooka, T. Hosoya, *Org. Lett.* **2018**, *20*, 4126.

[22] M. Julino, U. Bergsträßer, M. Regitz, *Synthesis (Stuttg).* **1996**, *1996*, 87.

[23] G. L. Hillhouse, G. V. Goeden, B. L. Haymore, *Inorg. Chem.* **1982**, *21*, 2064.

[24] G. L'abbé, *Chem. Rev.* **1969**, *69*, 345.

[25] G. Smolinsky, E. Wasserman, W. A. Yager, *J. Am. Chem. Soc.* **1962**, *84*, 3220.

[26] E. Niecke, D. Gudat, E. Symalla, *Angew. Chemie* **1986**, *98*, 817.

[27] W. S. Holmes, *Trans. Faraday Soc.* **1962**, *58*, 1916.

[28] A. H. Woomer, T. W. Farnsworth, J. Hu, R. A. Wells, C. L. Donley, S. C. Warren, *ACS Nano* **2015**, *9*, 8869.

[29] F. Tao, Z. H. Wang, X. F. Chen, G. Q. Xu, *Phys. Rev. B* **2002**, *65*, 1.

[30] M. Newville, T. Stensitzki, **2014**, DOI 10.5281/zenodo.11813.

[31] F. L. Lin, H. M. Hoyt, H. van Halbeek, R. G. Bergman, C. R. Bertozzi, *J. Am. Chem. Soc.* **2005**, *127*, 2686.

[32] L. N. Karyakina, a. V. Oleinik, *High Energy Chem.* **2010**, *44*, 498.

[33] G. Socrates, *Infrared and Raman Characteristic Group Frequencies: Tables and Charts*, Wiley, Chichester, **2004**.

[34] S. Yang, Y. Liu, P. Gao, T. Zhang, X. Zhu, M. Zhang, M. Chen, P. Du, G.-W. Wang, H. Ji, J. Yang, *Angew. Chemie Int. Ed.* **2018**, DOI 10.1002/anie.201813218.

[35] J. F. Moulder, W. F. Stickle, P. E. Sobol, K. D. Bomben, *Phys. Electron. Inc., Eden Prairie, Minnesota* **1992**, DOI 10.1002/sia.740030412.

[36] W. M. Holden, O. R. Hoidn, A. S. Ditter, G. T. Seidler, J. Kas, J. L. Stein, B. M. Cossairt, S. A. Kozimor, J. Guo, Y. Ye, M. A. Marcus, S. Fakra, *Rev. Sci. Instrum.* **2017**, *88*, 73904.

[37] W. M. Holden, O. R. Hoidn, G. T. Seidler, A. D. DiChiara, *Rev. Sci. Instrum.* **2018**, *89*, 93111.

[38] H. Lu, V. Subbarayan, J. Tao, X. P. Zhang, *Organometallics* **2010**, *29*, 389.

[39] S. C. Hockey, G. J. Barbante, P. S. Francis, J. M. Altimari, P. Yoganantharajah, Y. Gibert, L. C. Henderson, *Eur. J. Med. Chem.* **2016**, *109*, 305.

[40] P. Trillo, H. Adolfsson, T. Slagbrand, A. Volkov, F. Tinnis, *ACS Catal.* **2017**, *7*, 1771.